Design of MEMS Based Universal Testing Machine for Thin Film Characterization

Author

Arslan Ul Haq

00000171745

Supervisor

Dr. Muhammad Mubasher Saleem

DEPARTMENT OF MECHATRONICS ENGINEERING

COLLEGE OF ELECTRICAL & MECHANICAL

ENGINEERINGNATIONAL UNIVERSITY OF SCIENCES AND

TECHNOLOGY

ISLAMABAD

August, 2020

Design of a MEMS Based Universal Testing Machine for Thin Film Characterization

Author

ARSLAN UL HAQ

00000171745

A thesis submitted in partial fulfillment of the requirements for the degree of

MS Mechatronics Engineering

Thesis Supervisor:

DR. MUHAMMAD MUBASHER SALEEM

Thesis Supervisor's Signature: ____________________________________

DEPARTMENT OF MECHATRONICS ENGINEERING
COLLEGE OF ELECTRICAL & MECHANICAL ENGINEERING
NATIONAL UNIVERSITY OF SCIENCES AND TECHNOLOGY,
ISLAMABAD
August 2020

Declaration

I indorse that this research work titled "*Design of a MEMS Based Universal Testing Machine for Thin Film Characterization*" is my own work. The material used in this work from other sources has been properly referenced and it hasn't been presented elsewhere for assessment.

Signature of Student
Arslan Ul Haq
00000171745

Language Correctness Certificate

This thesis has been read by an English expert and is free of typing, syntax, semantic, grammatical, and spelling mistakes. The thesis is also according to the format given by the university.

Signature of Student
Arslan Ul Haq
00000171745

Signature of Supervisor

Copyright Statement

Acknowledgements

I am really thankful to Allah the Creator for great blessing during this time of struggle and for keeping me motivated all the time. Without His blessing it was really impossible for me to accomplish this task.

I am also thankful to my beloved siblings who supported continuously throughout this journey. Especially to my elder brother who kept me motivated and supported me financially.

I would also like to express special thanks to my supervisor Dr. Muhammad Mubasher Saleem for creating a passion in me to opt for the field of MEMS and helping me throughout my thesis. Also, he guided and motivated me to enhance my research for the betterment of MEMS community. I pay my gratitude to Dr. Amir Hamza, Dr. Danish Hussain and Muhammad Saqib for their tremendous support, guidance and cooperation. Without their help, I wouldn’t have been able to complete my thesis.

Finally, I would like to express my thankfulness to all the characters that have rendered valuable assistance to my study.

Dedicated to my exceptional family members, friends, and teachers

Abstract

Many materials now a day used in Micro Electromechanical Systems (MEMS) were not considered as mechanical material before. So their mechanical properties are not well known which are very important to predict their specifications like sensitivity, range, and the life which are very important for their reliability. These materials are used in many real time-critical applications where a minor error can cause serious damage just like the accelerometer used for impact detection in automobiles to activate airbags. Thus the mechanical properties should be exactly known then we can define the device characteristics. Similarly, many other applications like in aviation, aerospace, and telecommunication, etc. The mechanical properties of the material used in the MEMS devices should be exactly known for their reliable and safer use. Out of these mechanical properties yield strength of a material has a critical role in the response of a device. There are many challenges in material testing at micron level like the generation of force with such fine resolution, load sensing, adjustment of the specimen, etc. Most of the researchers have used a monolithically fabricated specimen with a testing mechanism that limits the type of test materials. Secondly, for separately fabricated specimens the mounting and collection of specimens to the test structure before and after the test is a challenge. The main objective of this thesis is to design a generalized MEMS-based testing machine that can find the yield strength of different thin films at the MEMS level. The main focus of our work is to make the load application and sensing the more reliable and easier. The biaxial testing mechanism in used with Chevron type electrothermal actuator for force application and gap, an anti-gap capacitive sensor to find the yield strength. The proposed design is validated through FEM analysis on ANSYS.

Key Words: *MEMS, FEM, Electrothermal actuator, Capacitive sensor, Tensile Testing, Specimen, Stress, Strain, Deformation, Temperature rise, Yield stress.*

Table of Contents

List of Figures

List of Tables

Acronyms

MEMS	Microelectromechanical Systems
ETA	Electro Thermal Actuator
FEM	Finite Element Method

Chapter 1: Introduction

This chapter has two parts. The first one deals with an introduction of MEMS (Microelectromechanical systems) and the working principle of the MEMS testing machine. The second one deals with prior work in the testing of mechanical properties in MEMS.

1.1 A Brief History of MEMS

MEMS (Microelectromechanical systems) is a broad term encompassing a vast range of batch fabricated products. Specifically, MEMS are any devices that use both electrical and mechanical structures ranging from micrometer to centimeter scale. In its conventional sense, MEMS technology is categorized by its flexibility to fabricate and integrate an extensive range of electromechanical components to implement a complete system on the micro-scale that can perform tasks in a way comparable to macroscopic devices. MEMS utilizes the microfabrication technology used in semi-conductor industries for the development of integrated circuits (IC's). The most important steps in the fabrication of IC's consist of ion implantation, epitaxial growth, physical vapor deposition, chemical vapor deposition, and etching, evaporation, and electrodeposition of metals. MEMS devices use the same fabrication steps with the exception that the sequence of steps may vary from application to application. The process of lithography is used to determine the areas of the structure undergoing the previously mentioned fabrication steps[1].

MEMS emerged in the IC industry in the mid-1960. One of the very first micromechanical device was invented by H.C Nathanson [2]. By the early 1980s, MEMS devices grew in popularity due to improvements in the processing and fabrication technologies. A significant amount of research is done by Howe and Muller in 1983 by the fabrication of suspended microcantilever and micro bridges using silicon dioxide as a sacrificial layer [3]. Since then an extensive variety of MEMS-based mechanisms and devices are fabricated that are replacing their traditional counterparts in automotive, aerospace, optics, energy, data storage, and biomedical industries [4] due to their small size, low cost, improved performance, and simpler structures [5] figure 1.2 shows the most prominent application areas of MEMS technology.

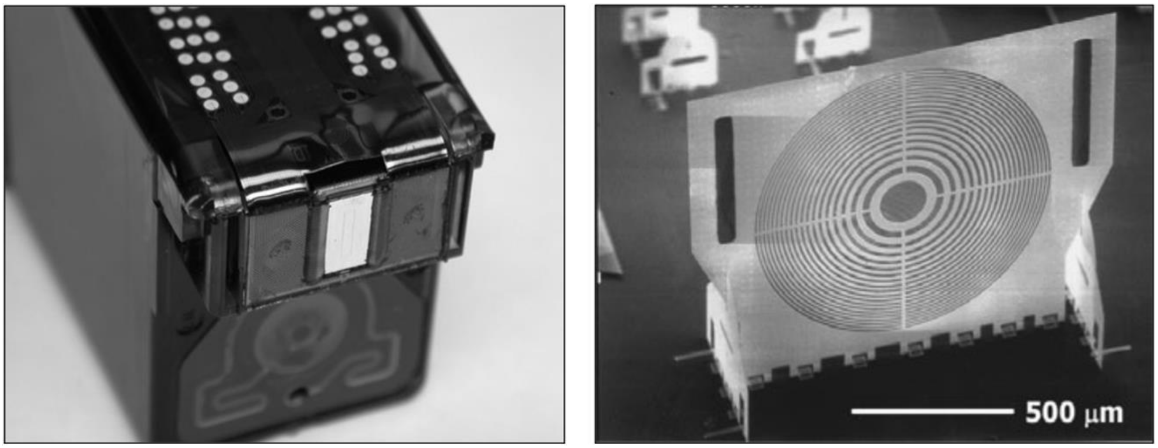

Figure 1.1: MEMS ink jet chip (left), MEMS binary lens (right) [4].

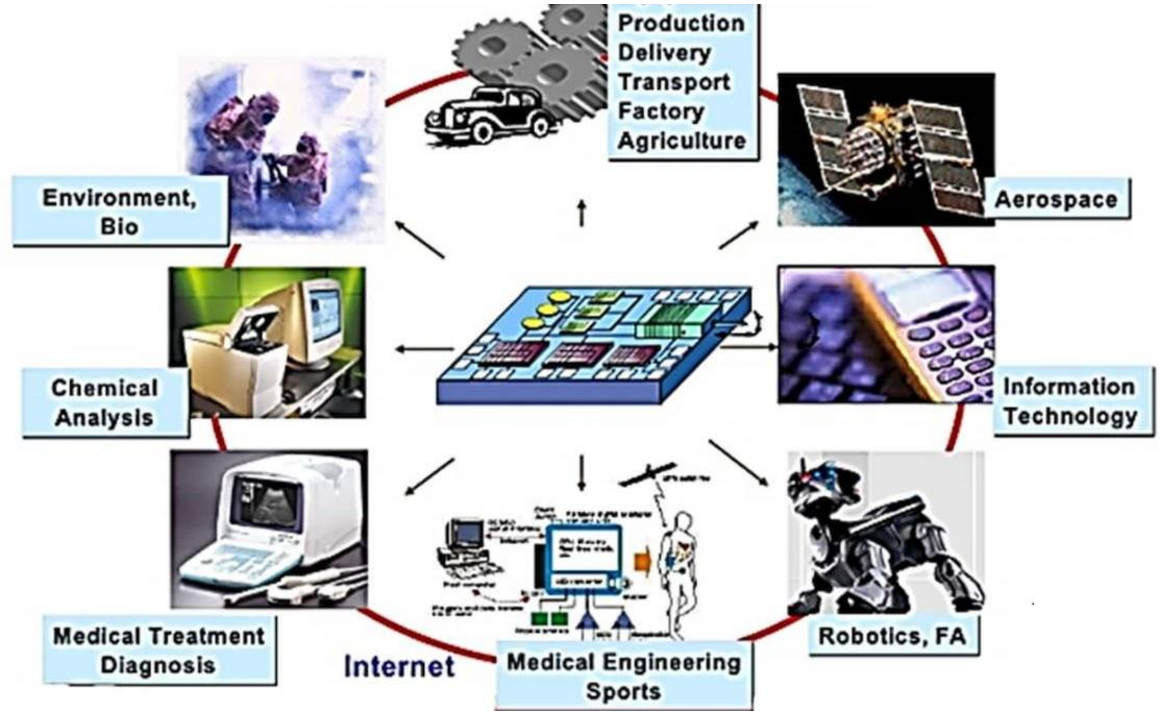

Figure 1.2: Application of MEMS devices/systems [6].

Apart from these, MEMS microfabrication processes are also revolutionizing the field of commercial and military communication systems, microwaves, and satellite systems by the demonstration of a wide range of lumped components like capacitors, inductors, and micro relays. These components then combined to form complex systems like filters, resonators, switching networks, antennas, and phase shifters [6].

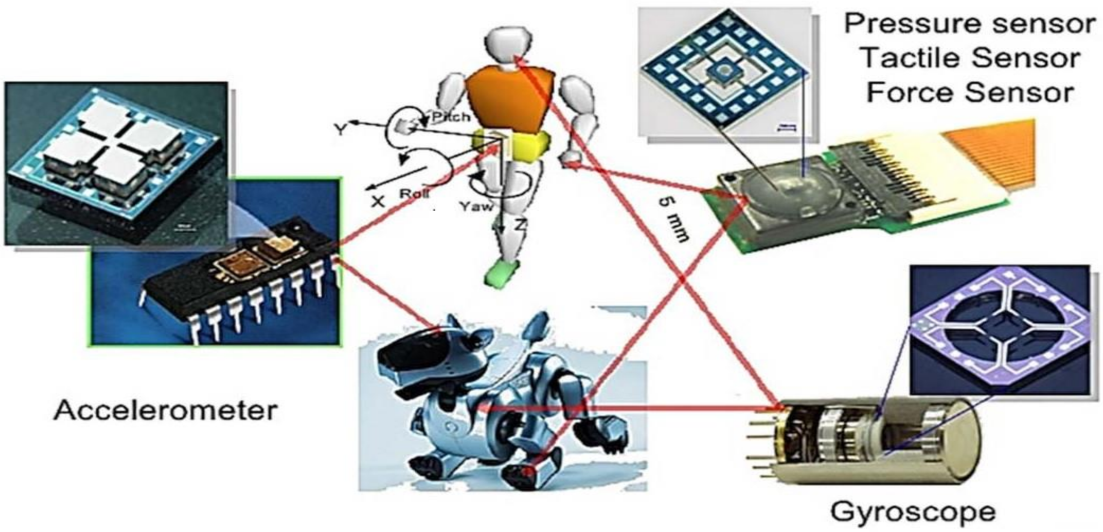

Figure 1.3: Applications of MEMS devices/systems [6].

1.2 Tensile Testing Principle

The tensile testing machine may be uniaxial or biaxial but both give almost the same results. In uniaxial on end if fixed and force is applied from the other end and in biaxial force is applied from both ends of the specimen [7]. And a stress-strain graph is drawn to measure the different mechanical properties of a material.

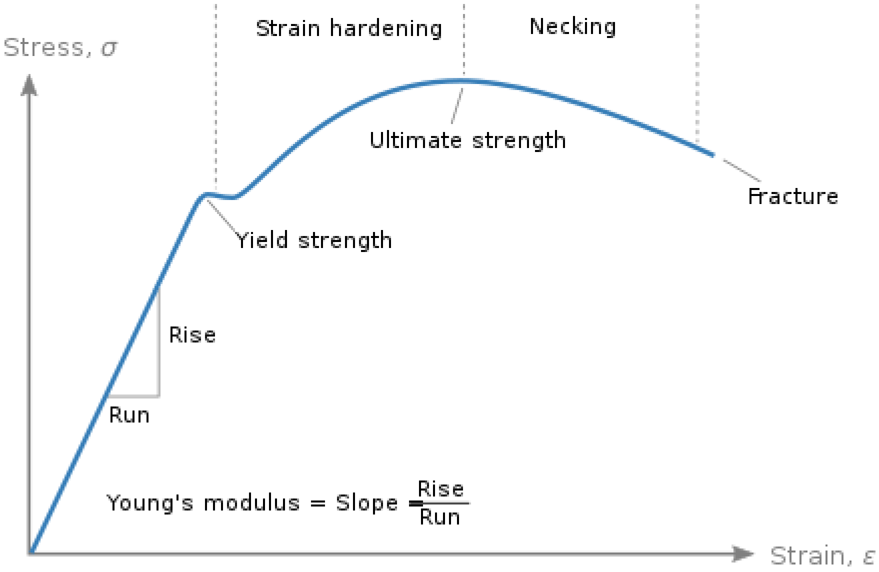

Figure 1.4: A stress-strain curve for tensile testing [8].

1.3 Prior Work of MEMS Material Testing

Electrothermal, electrostatic, piezoelectric, and electromagnetic are major actuation techniques used in material testing in MEMS. We will concisely discuss all four actuation techniques to investigate application areas and previous research.

Toshiyuki et al. [9] used electrostatic force for gripping the specimen and conduct the *in-situ* observation inside the SEM chamber and tested the samples of polycrystalline silicon ranging from 30-300µm long, 2-5µm wide and 2µm thick. They found the tensile strength depends upon the length of the specimen, not on the specimen width.

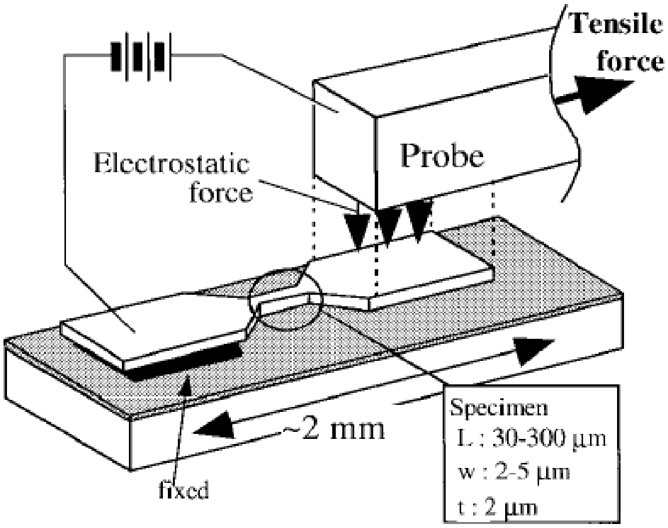

Figure 1.5: Electrostatic force for actuation [9].

M.T.A Saif et al. [10] design two micro-instruments for the characterization of submicron scale material. Out of these one was used for torsion test of a square cross-sectional area bars of silicon until fracture. And found the 5.6 and 2.6 GPa shear stress before the fracture. The second one used tensile testing of a composite of aluminum and silicon dioxide beam of 1 × 1.5 μm^2 cross-section area. They found the beam fail at 200µN. The used electrostatic comb drive for actuation.

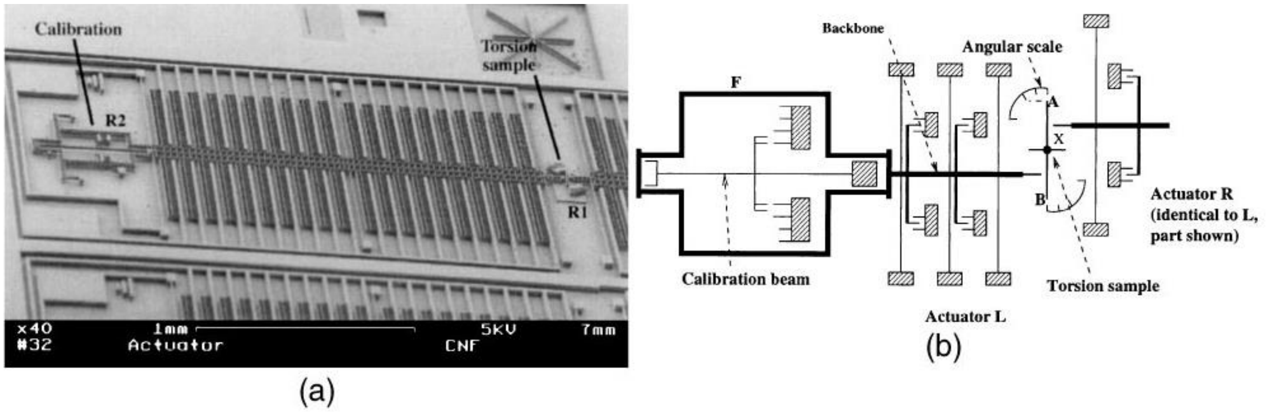

(a) (b)

Figure 1.6: (a) SEM image for microinstrument of torsion test (b) Schematic top View [10].

M. A. Haque and M. T. A. Saif [11] used a load sensor and specimen which are fabricated on the same chip. This chip includes a load beam designed according to the required force resolution attached to the specimen with a supporting structure. The chip has two holes one for fixing and another for actuation force application. Different types of materials like metals, dielectrics, and multilayers composites that can be grown on silicon composites can be tested by this mechanism at the micron and submicron level. The force resolution can be controlled by the spring constant of the load cell beams. Elongation in the specimen is measured by the markers on it in the SEM.

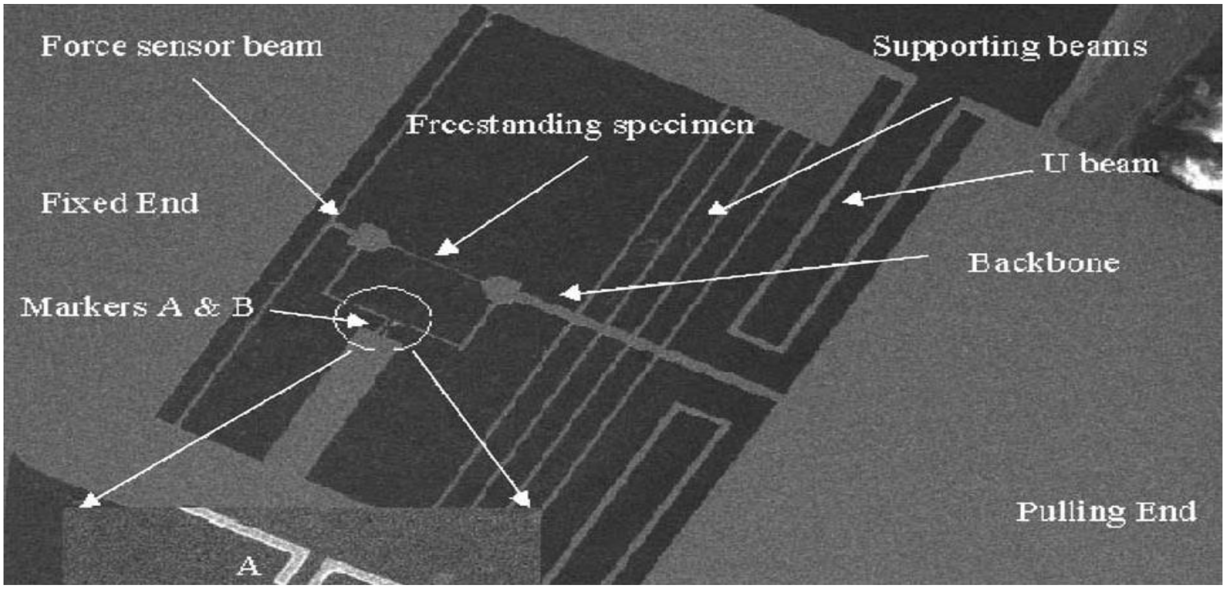

Figure 1.7: Cofabricated specimen and load cell in the test chip [11].

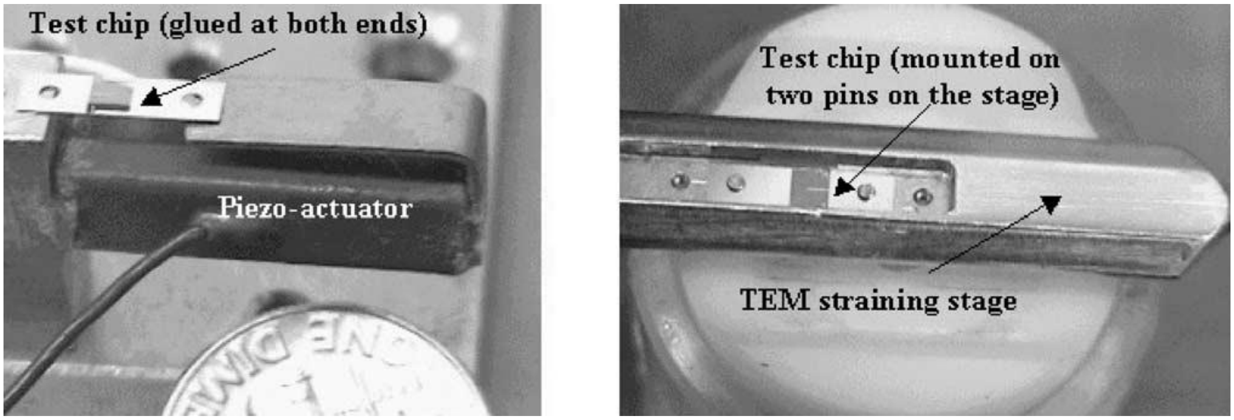

Figure 1.8: Experimental setup for in situ tensile testing inside SEM [11].

I. Chasiotis and W. G. Knauss [12] demonstrated a novel technique for measuring Young's modulus, Poisson's ratio, and tensile strength of the polysilicon specimen. Atomic Force Microscopy (AFM) was used to measure the topology of the specimen under deformation and digital image correlation method to find the strain and inchworm actuator used to apply the load. powered by personal computer through a dedicated controller. A load cell used to measure the load

M. A Haque and M. T. A. Saif [13] developed a setup for single and multilayer specimens that can be fabricated separately from the rest of the structure. Specimens can be fabricated at both micron and submicron levels. They used a microgripper to grip the specimen and once the gripper and the specimen are aligned the whole assembly is put inside the SEM. The actuation force is generated by lateral comb drive which can generate a maximum load of 383 µN with the resolution of 3 nN.

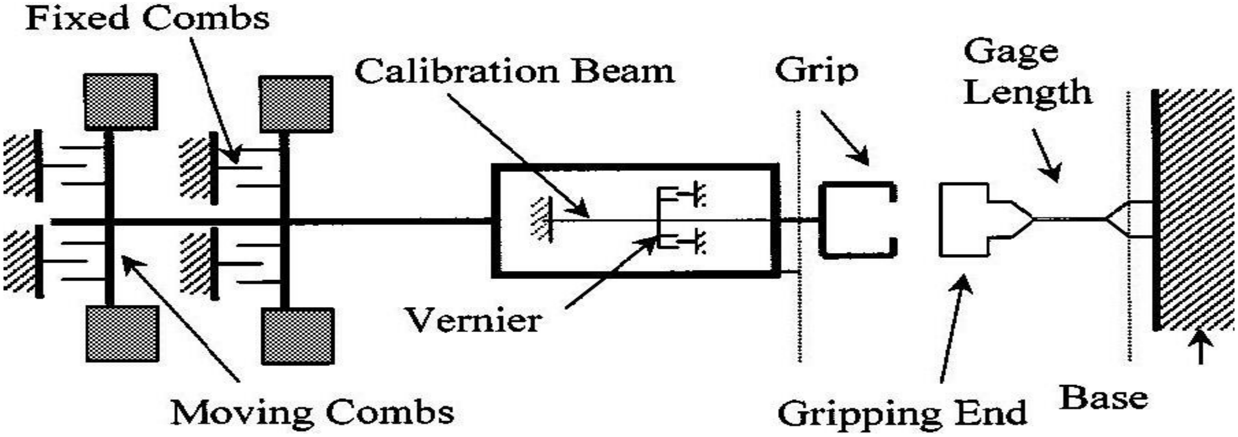

Figure 1.9: A Schematic of tensile testing setup with comb-drive actuator and gripper [13].

Y. Ison et al. [14] tested the specimen of diamond-like carbon (DLC) which is used to protect the MEMS devices against wear and friction. Atomic force microscopy (AFM) tensile test and nano-indentation test were used to measure Young's modulus and the Poisson's ratio of a 2 μm to 3 μm thick layer of DLC on a single crystalline silicon specimen.

T. Tsuchiya [15] investigated the origin of fracture by statistical analysis and strength of nanometer-thick film with help of an electrostatic gripper, a piezoelectric actuator to apply the load, a load cell to measure the load, and the strain was measured with the help of images analysis technique by used marked images of the specimen.

S. W. Han et al. [16] used a specimen gripper to glued the specimen on the piezoelectric actuator. The strain is measure directly with the help of ISDG a laser interferometer technique. The stress-strain curve, elastic modulus, and ultimate tensile strength were found with the help of this technique.

A. V. Desai and M. A. Haque [17] design a silicon chip with a piezoelectric actuator for mechanical testing of nanowire and nanotubes. They tested a ZnO nanowire using Focused Ion Beam Systems (FIB) to estimate the fracture strain of ZnO nanowire. A silicon chip is mounted on a piezoelectric actuator. Then the voltage is applied to the piezoelectric actuator and a crack is developed on the chip the nanowire with its solution is mounted on the crack perpendicularly and again the piezoelectric actuator is activated and again a crack is developed in the nanowire. The applied load is measure by the applied voltage to the load and elongation in the nanowire is estimated by the FIB system and crack strain is measured.

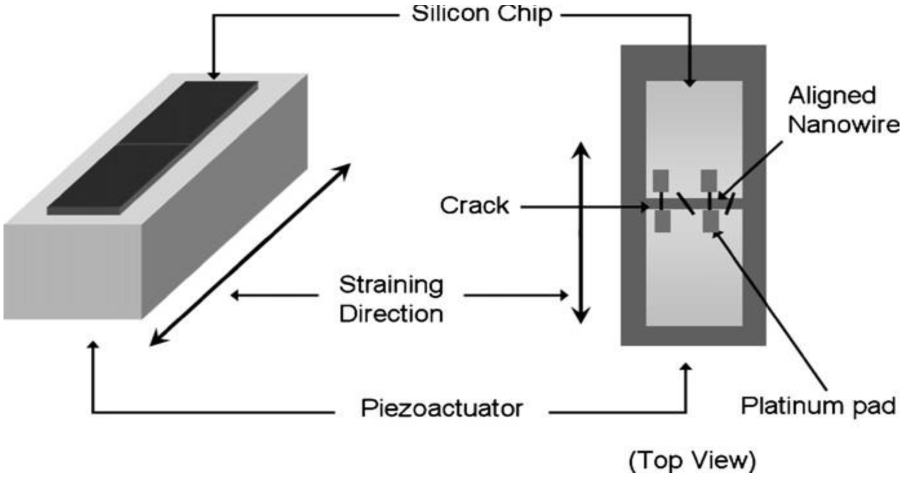

Figure 1.10: A schematic of the straining experimental setup [17].

Y. Zhu et al. [18] designed a MEMS-based material system that consists of a V-shaped thermal actuator for the force application and a capacitive load sensor. A specimen can be fabricated monolithically with the system or it can be fixed in the system by nano manipulator inside the TEM. A variety of different material specimens a range from micron to submicron level can be tested by this system. The load is applied by applying the voltage to the thermal actuator which can be designed with different ranges by changing simply the number of beams and beam angle and load on the specimen is measured by the capacitive load cell.

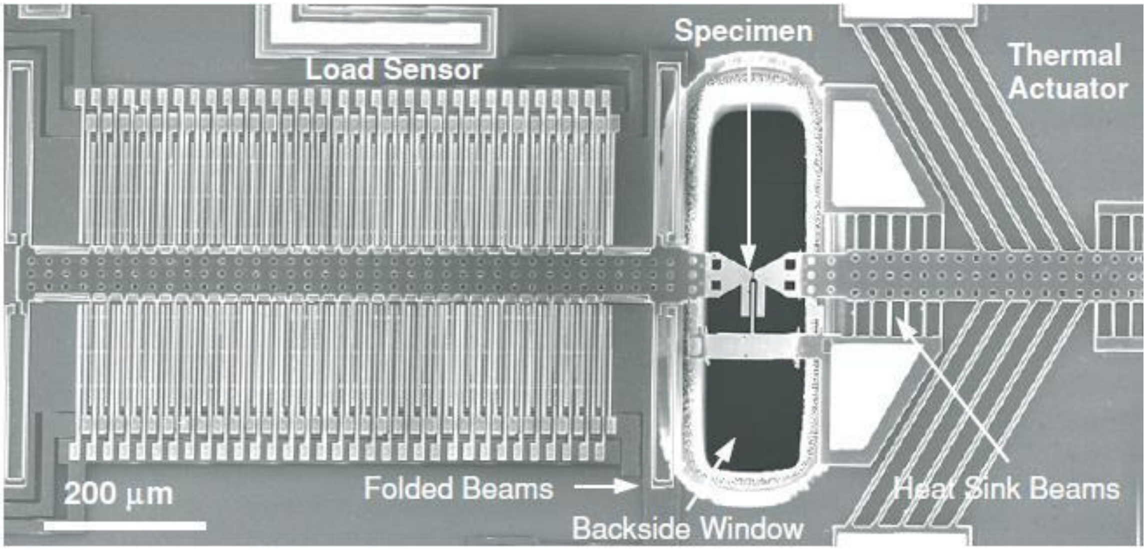

Figure 1.11: MEMS-based material testing system with a thermal actuator, a load cell, and a specimen [18].

H. D. Espinosa et al. [19] used a similar design as used by Y. Zhu et al. [18] but they fabricated the specimen monolithically with the test system and used both electrothermal and electrostatic actuation processes for force application. Electrostatic actuation has a large footprint but small actuation power and no heat transfer to the specimen. In the case of the electrothermal actuation process, they used heat sink beams to avoid the heat transfer to the specimen. But in the case of electrothermal actuation, the generated force is much more as compared to the electrostatic. A detailed comparison of both electrothermal and electrostatic actuation processes for load application is given.

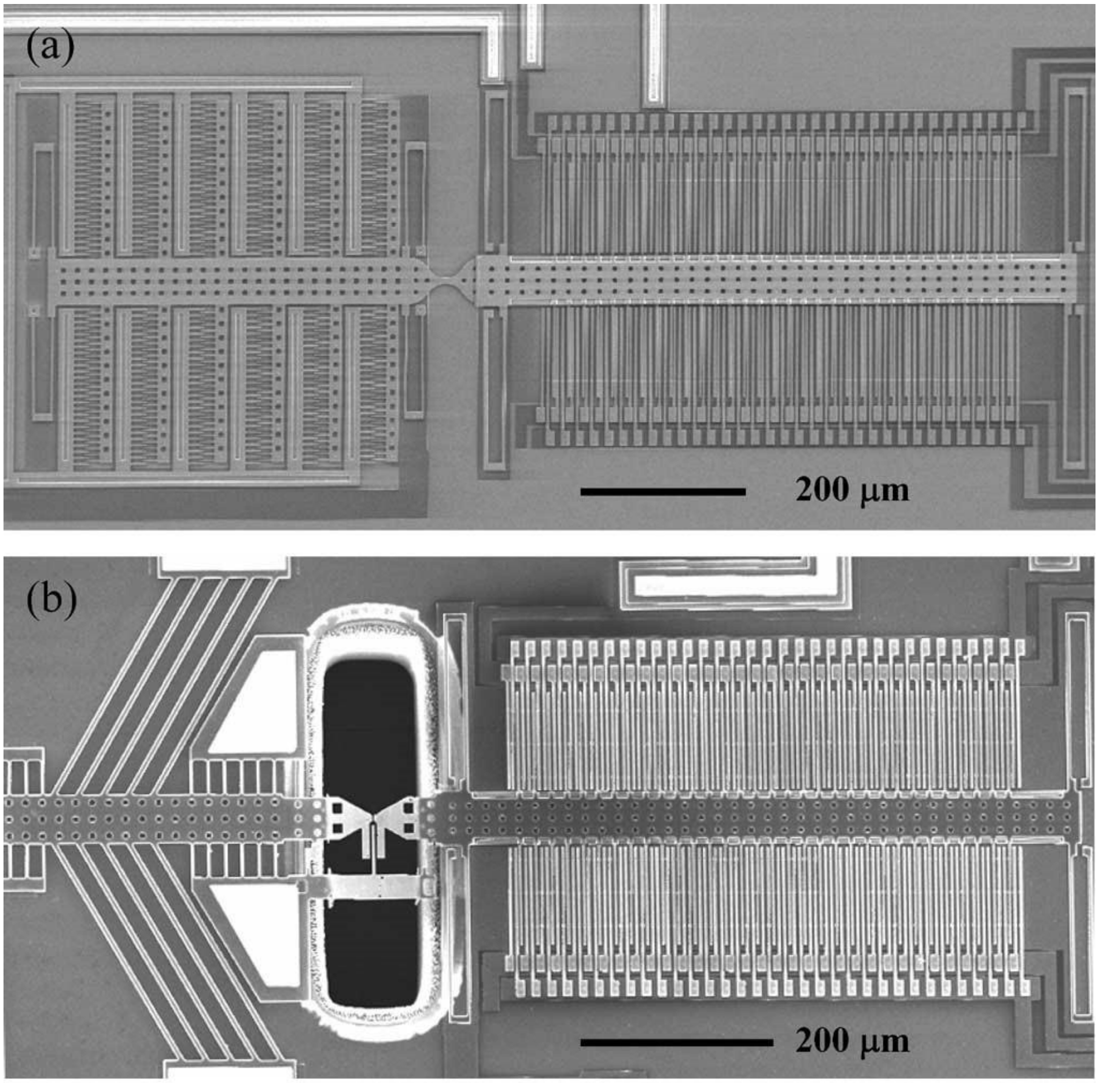

Figure 1.12: (a) MEMS-based material testing systems with a thermal actuator, a load cell, and a specimen (b) MEMS-based material testing systems with an electrostatic actuator, a load cell, and a specimen [19].

J. H. Han et al. [20] developed a stage in the dimension of millimeters which consists of bending beams for the load measurement and the markers for the strain measurement. The specimen is mounted on the stage with help of glue and the stage is stretched by a piezoelectric actuator and both load and strain are measured from the load cell and the TEM images.

M. Naraghi et al. [21] designed a novel MEMS system for the mechanical characterization of nanofibers which are highly deformable. They used leaf spring as a load sensor and an external piezoelectric actuator as a source of actuation. The whole system is kept under the optical microscope which measures the deformation in the leaf spring and the elongation in the specimen used to measure the stress and the strain. The atomic force microscopy (AFM) cantilever is used for gripping the specimen beam by an adhesive application.

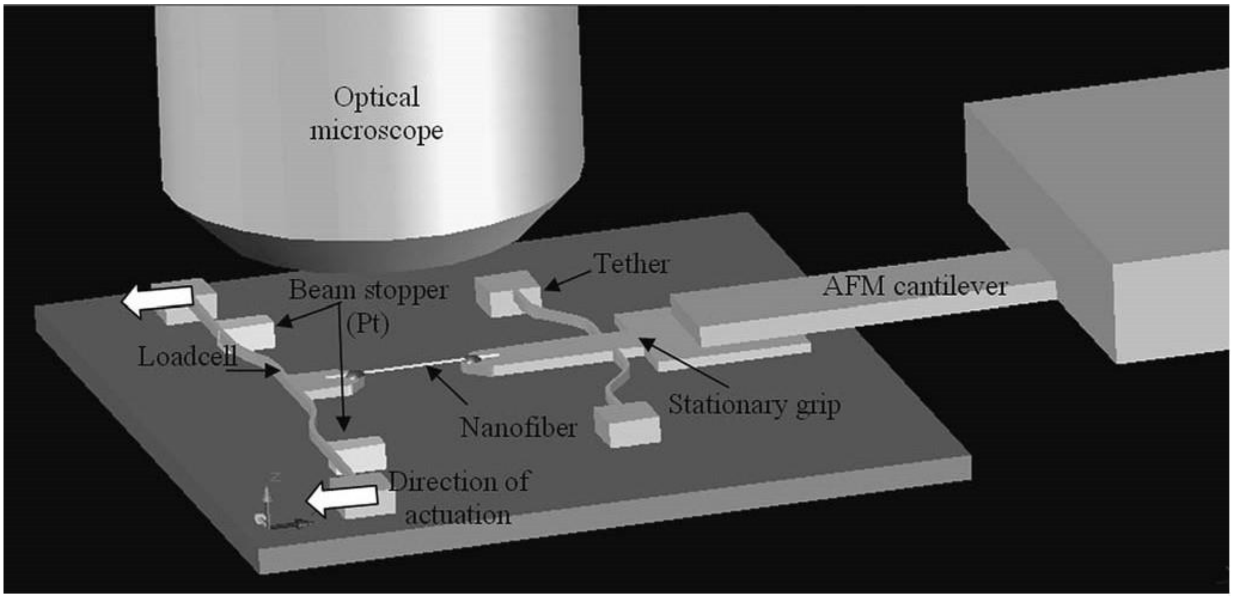

Figure 1.13: Application of the test platform for nanofiber testing [21].

Q. H. Han et al. [22] designed a MEMS-based system for tensile testing at the submicron level which consists of an electrostatic actuator, a load cell beams, and a 90 nm thick specimen of single crystalline silicon. The load is applied by the electrostatic actuator, measured by the load cell, and the strain is measured by the TEM images to plot the stress-strain curve.

J. Ha et al. [23] used a novel non-contact technique to measure stress and strain with the help of a CCD camera from the imaging of the indicator on the guide side and the specimen side. They used four indicators on the guide side and four on the specimen side which are not affecting the deformation of the specimen. An electromagnetic actuator is used to pull the specimen from the movable side and on another end is fixed with the load cell beams which are deflecting according to the applied load. They also used a capacitance type deflection meter between the fix and movable end of the specimen.

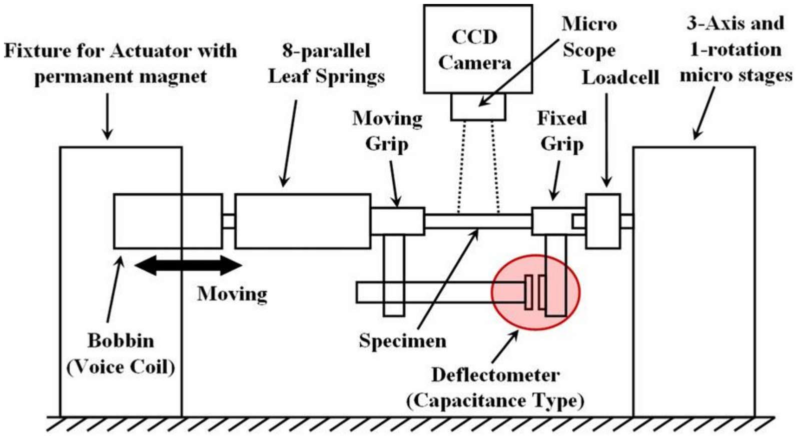

Figure 1.14: A schematic view of the proposed system [23].

R. Liu et al. [24] used a separately fabricated specimen frame with the spring supported structure and apply actuation force with a piezoelectric motor. The used a nickel frame with an s-type spring to supports. The adjustable frame has a hole inside to adjust with the actuation motor. The whole structure is placed under a microscope equipped with CCD on an adjustable table which has adjustment along x-y-z-θ. A laser displacement sensor having a transmitter, receiver, and display is used to measure the elongation, and a force sensor is used for load sensing. The piezoelectric motor generate displacement with a resolution of 0.02μm.

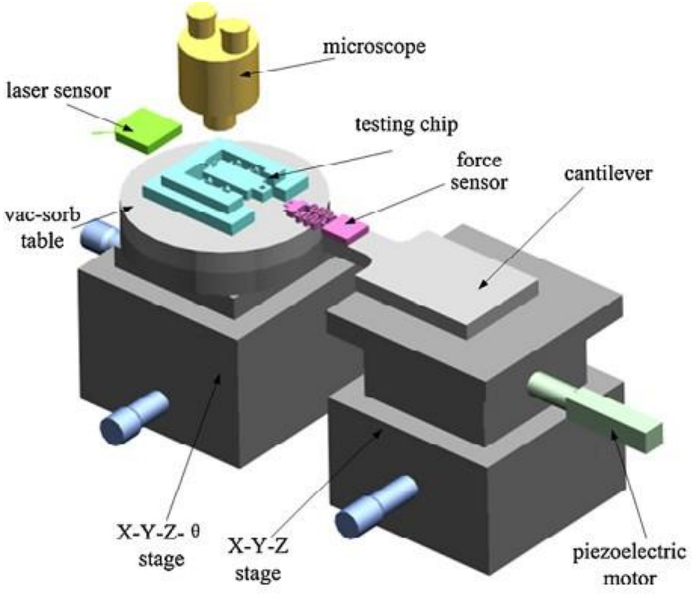

Figure 1.15: A schematic of the test setup [24].

J. Brown et al. [25] used an electrothermal actuator for actuation force, piezoelectric load beams for the load sensing, and diffraction grating for the displacement sensing. A V-shaped electrothermal actuator is used for uniaxial pulling of the specimen which is attached to piezoelectric beams which are bending directly proportional to the applied load. A diffraction grating is used on the opposite side of the specimen from which with microscopic interpretation strain data is collected.

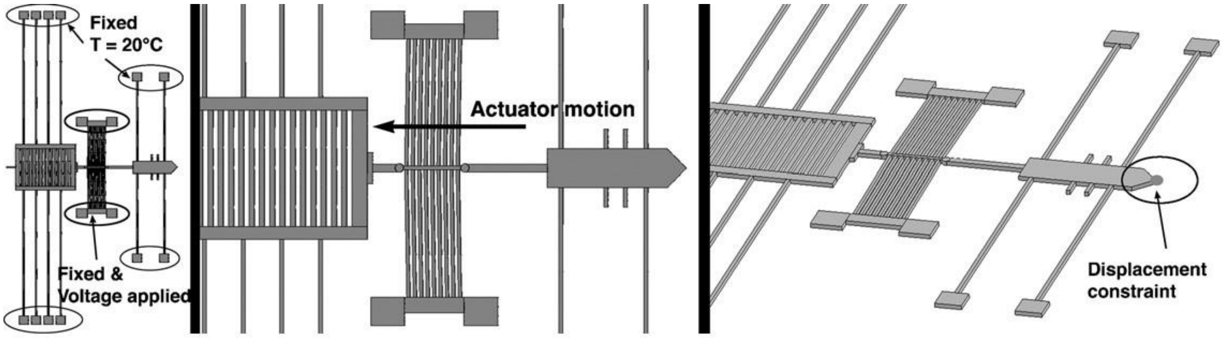

Figure 1.16: A schematic of the design with an electrothermal actuator, spring, and large grating [25].

F. Schneider et al. [26] used German Industry Standard DIN53504 [27] to test the Polydimethylsiloxane (PDMS) which is used to embed and encapsulate the electronic component which increases their life span, the tear strength. The tensile strength, the strain, and the stress values at the breakpoint. DIN53504 is used to test the rubbers and elastomers. They developed four different samples with different gauge lengths and used the machine to test these samples one by one in different modes of operation.

Y. Gansean et al. [28] developed a specific design for the testing of a nanowire of nickel. They used a nanoindenter for load application and SEM/TEM for the measurement of deformation. A nanowire of nickel is attached to the two moveable shuttles supported by the eight inclined beams. The shuttles are free to move in x-axis direction under loading. The supported beams are inclined at the angle of 45° to transfer the maximum load to the specimen. Nanoindenter from the top of the shuttle applies the load which is transferred through inclined beams to the specimen and moveable shuttles move in the opposite directions along the x-axis and stress is developing in the specimen. Movement of the shuttles is measured from SEM/TEM and load from the nanoindenter. A stress-strain graph is plotted.

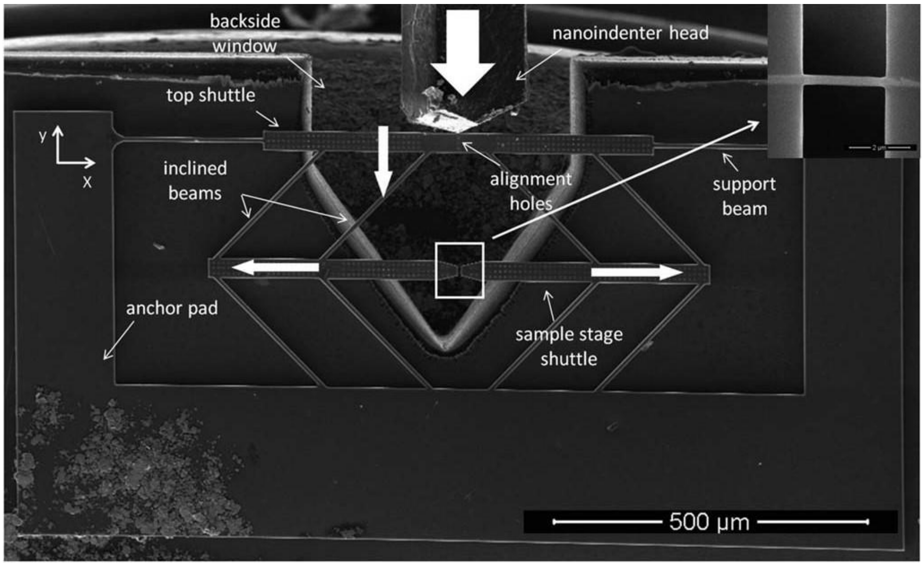

Figure 1.17: A SEM image of the microdevice and its components [28].

W. Kang et al. [29] investigated the effects in the results due to the specimen misalignment during the tensile testing and developed a novel technique for the specimen mounting to reduce the misalignment. A testing stage is designed with a set of load sensing and supporting beams having two pinholes at both ends one for fixing and another for the force applicator. A dog-bone shaped specimen is fabricated to mount in between the grips. A piezoelectric actuator is used to pull the moveable end and stress is developed in the specimen. The SEM is used to measure developed stress and strain. A variety of material and size specimens can be tested by this technique without any misalignment error.

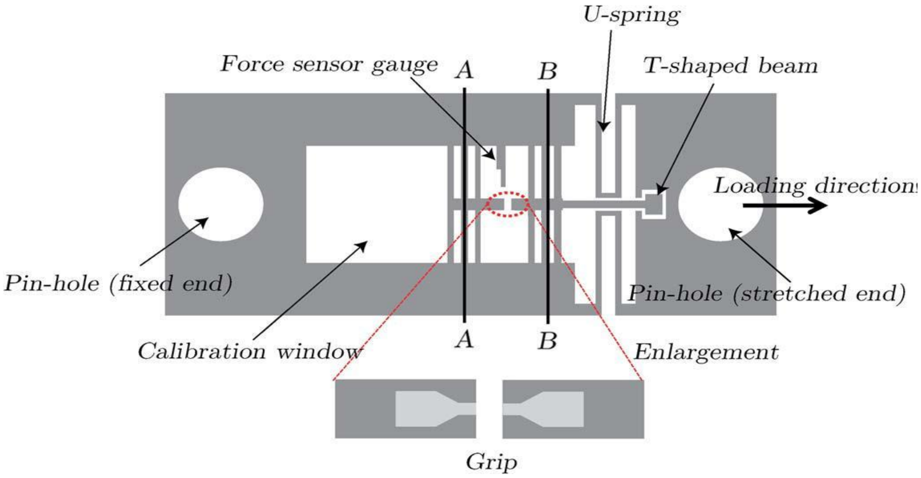

Figure 1.18: A schematic of the uniaxial stage for specimen alignment [29].

A. Boe et al. [30] proposed a very simple system for tensile testing at the micron level. A highly stressed beam of silicon nitride at high temperature is used as an actuator and the specimen is glued to the beam from one end and fixed to the structure from the other. Several numbers of cursors are fabricated on both beam and the structure which are used to measure the displacement covered by the beam. And the force is directly measured from the beam.

Y. Zhang et al. [31] developed a device for uniaxial tensile testing of nanomaterials. The used a capacitive actuator in place of electrothermal to avoid the heat transfer to the specimen which affect the properties of the specimen during the test. An electrostatic actuator with a capacitive displacement sensor at one side and a capacitive load sensor with bending beams at the other side is designed such that a specimen is mounted in between the electrostatic actuator and the load sensor with the help of a nano manipulator from it grown structure in the SEM. A related electronics circuit and the system are mounted on the same chip. It gives a much better sampling rate as compared to electron microscopic imaging.

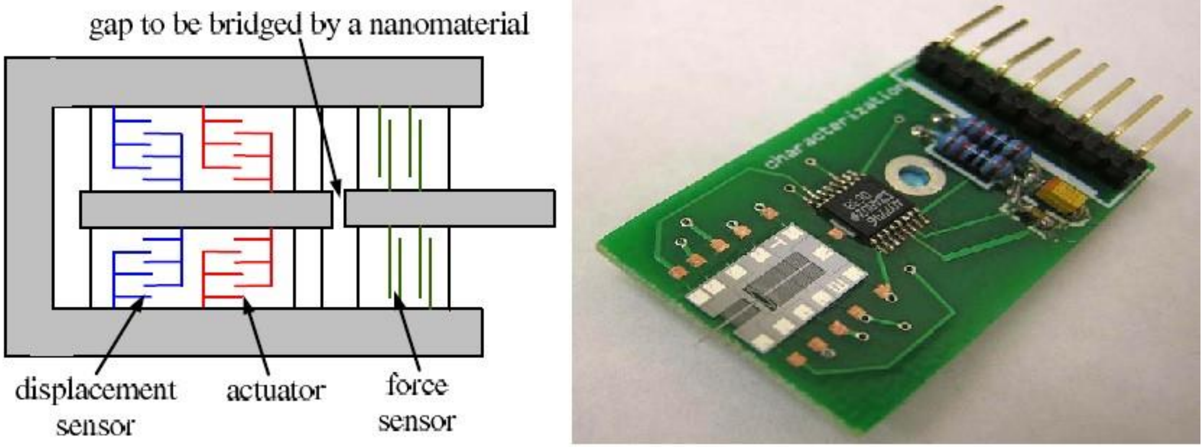

Figure 1.19: A schematic MEMS tensile testing stage device and circuit board [31].

Y. Lu et al. [32] used the same design as used by Y. Gansean et al. [28] with some modifications in the design to reduce the device size up to 3 mm × 2 mm to 2.5 mm × 1.2 mm for better fitting into the sample holder space which is highly restricted and decrease the device weight. Nickel nanowire is mounted on the test stage with the help of a nanoindenter inside the TEM.

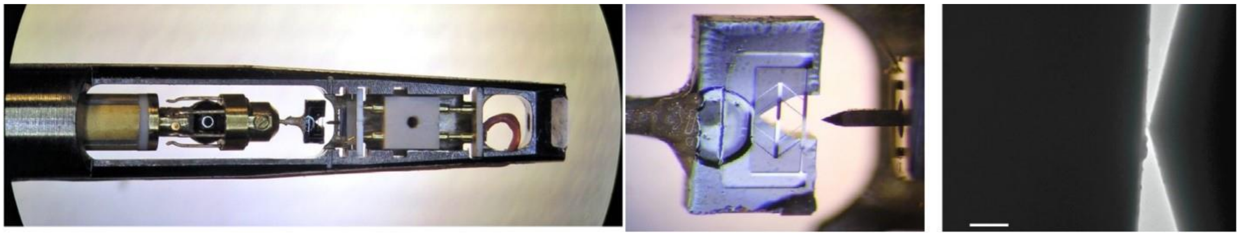

Figure 1.20: A view of the micromechanical device (MMD) and nanoindenter [32].

J. J. Brown et al. [33] developed a simple MEMS-based system for testing of gallium nitride nanowire by using an electrothermal actuator. The device was fabricated using the PolyMUMPS surface micromachining process consists of one fixed and one moving stage. The moving stage is connected to the electrothermal actuator and the specimen which is a nanowire is mounted between the two shuttles with the help of a nanomanipulator. The actuator is powered and the specimen starts deforming. The strain is measured directly from the SEM images and the force is measured by an indirect method. By subtracting the actual stage displacement with the specimen from the expected displacement of the stage without the specimen and multiplying with the spring constant of the system.

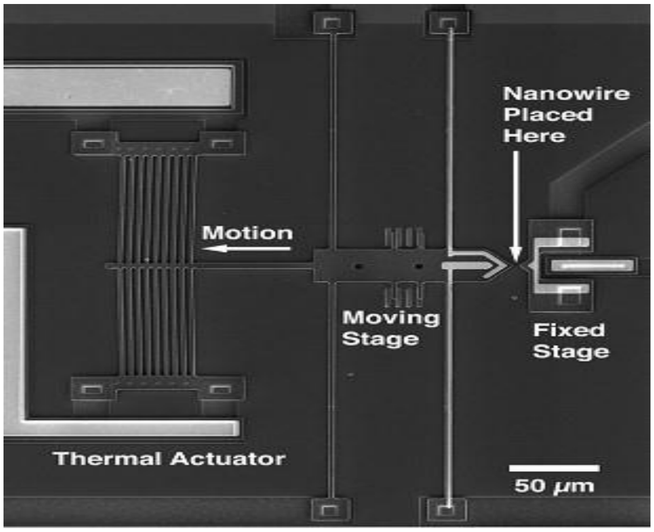

Figure 1.21: A view of the micromechanical device (MMD) and nanoindenter [33].

Z. H. Jiang et al. [34] designed a system to investigate the lattice behavior of silicon under tensile loading by using an electrostatic actuator to apply the load, a load cell for force sensing, and a TEM for imaging to find the strain and lattice behavior under different load values.

K. Abbas at al. [35] used a number cascaded electrothermal actuators system for testing of the platinum specimen. The system is capable of producing high pulling force in order of tens of milli-Newton with a displacement of tens of micron with a very low-temperature gradient. A nanowire of platinum is tested by this method which is fabricated monolithically in this case but can be fabricated separately and mounted in the system with help of nano manipulator and adhesive of the focus ion beam inside the SEM. Bending beams are provided to sense the applied load to the specimen. With the help of the SEM images and images correlation technique, the change in the specimen with an accuracy of < 10nm is measured. A very low-temperature gradient of less than 30^{o} C is achieved.

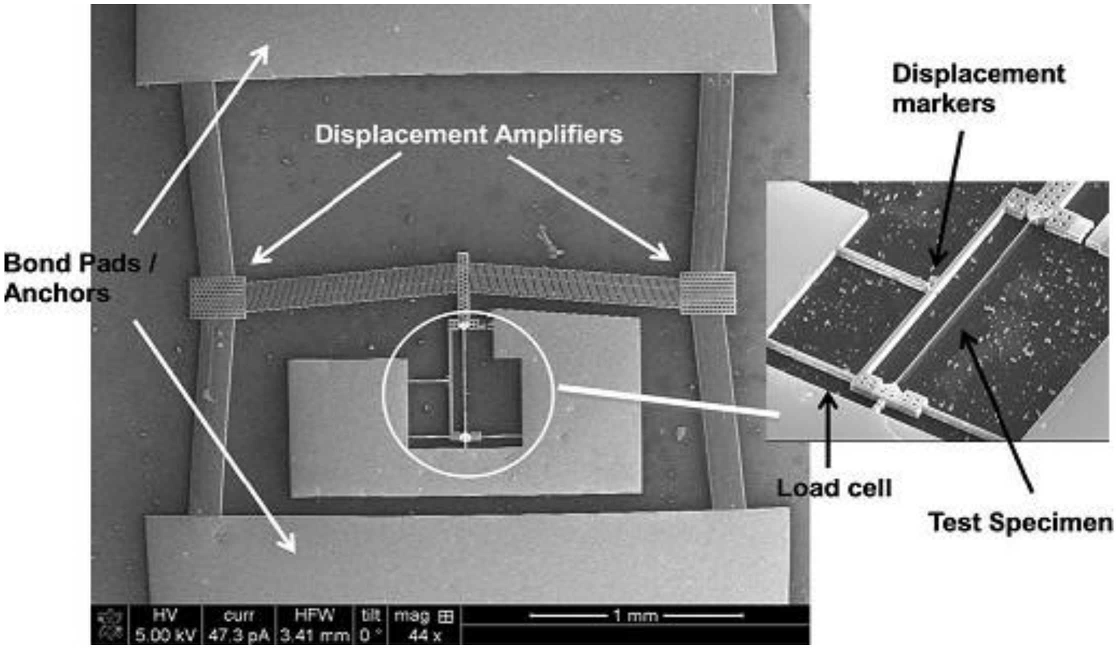

Figure 1.22: A SEM image of the cascaded thermal actuator system with a monolithically fabricated platinum specimen [35].

T. Tusachiya et al. [36] designed a system that can test nanomaterial by applying the force of nano newtons and the resolution of nanometers. A 16 µm long 2 µm wide and 40 nm thick wire is fabricated along with the system. Three comb drives are used in the series first one with the bending beams is used for the force measurement with a high resolution and the second one with supported beams is used for the displacement measurement and the last one is an electrostatic comb drive actuator which generates a force in the range of nano newton.

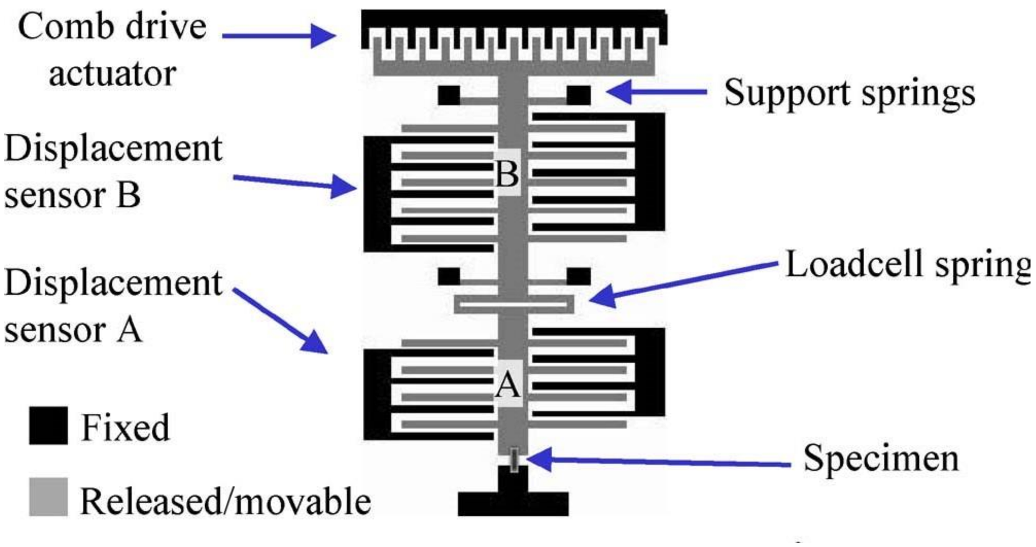

Figure 1.23: A schematic of the electrostatic tensile testing device [36].

M. Yilmaz and J. W Kaysar [37] developed a MEMS system for the characterization of the monolithically fabricated nanocrystalline gold specimen. To avoid the alignment issues in nanomaterial specimen testing which causes errors in the results. They fabricated a nanocrystalline gold specimen of 40 nm thick, 350 nm wide, and 6 μm with an electrostatic actuator and deflection beams for the load measurement. The test is performed in the SEM at room temperature. Digital image correlation software is used to measure displacement, stress, and strain. The ultimate tensile strength found by this method is 1GPa which is consistent with values found by other nanoscale material characterization techniques.

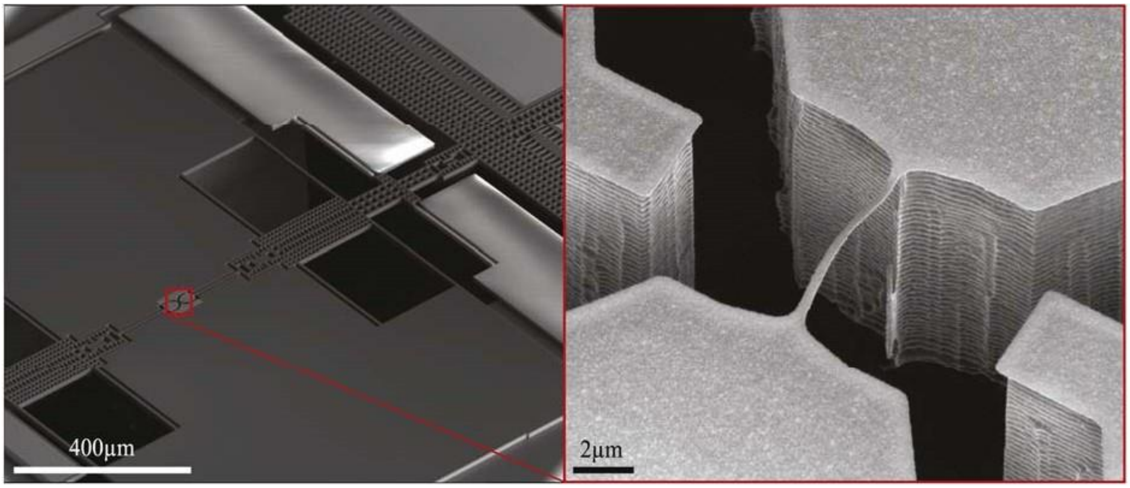

Figure 1.24: A SEM image of the testing device [37].

T. H. Chang and Y. Zhu [38] used a similar technique as used by Y. Zhu et al. [18] and H. D. Espinosa et al. [19] to test the monolithically fabricated specimen but additionally, they used two symmetrically fabricated electric heater on both sides of the test specimen to find the properties at different temperature. An electrostatic actuator is used to pull the specimen and a comb drive with deflection beams is used for load measurement. Due to the heater thermal elongation in the shuttle appear which creates compressive loads in the specimen to counter these additional electrothermal Z-shaped actuators are used on the opposite ends of the shuttles. Z-shaped actuators are used over the V-shaped due to their small central beams length which are easy in adjustment and have much lower stiffness comparatively.

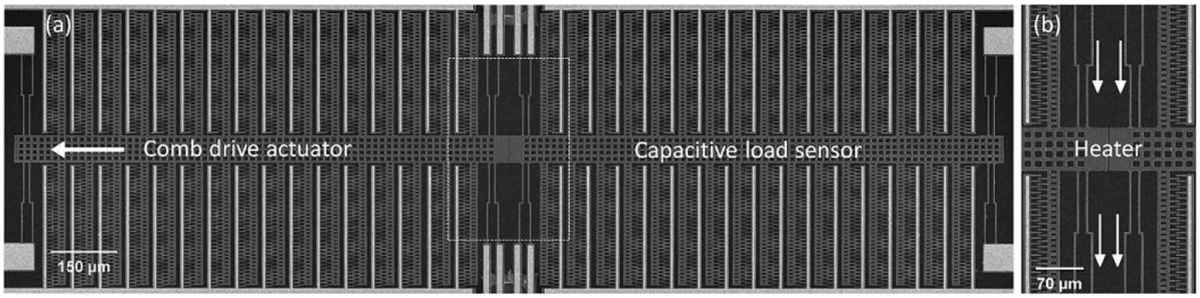

Figure 1.25: A SEM image complete MEMS testing device [38].

M. F. Patano et al. [39] designed a feedback system for the load sensor. A MEMS system for nanomaterial characterization with the comb drive actuators and a capacitive load sensor is fabricated. As the load sensor is fabricated with bending beams with a designed value of spring constant k according to the applied load. It is observed that in this kind of sensors an instability is shown when the specimen entering form the elastic to the plastic region specifically when the necking phenomenon starts the applied load decreases suddenly and the spring bounces back due to the stored energy. It creates an instability in the force measurement which causes an error. To control this type of error an additional electrostatic actuator is fabricated behind the load sensing comb drive which is connected to an electronics circuit design such as it always giving the feed of zero position according to the geometry and the applied voltage. So it avoids the error during the plastic region and the necking phenomenon.

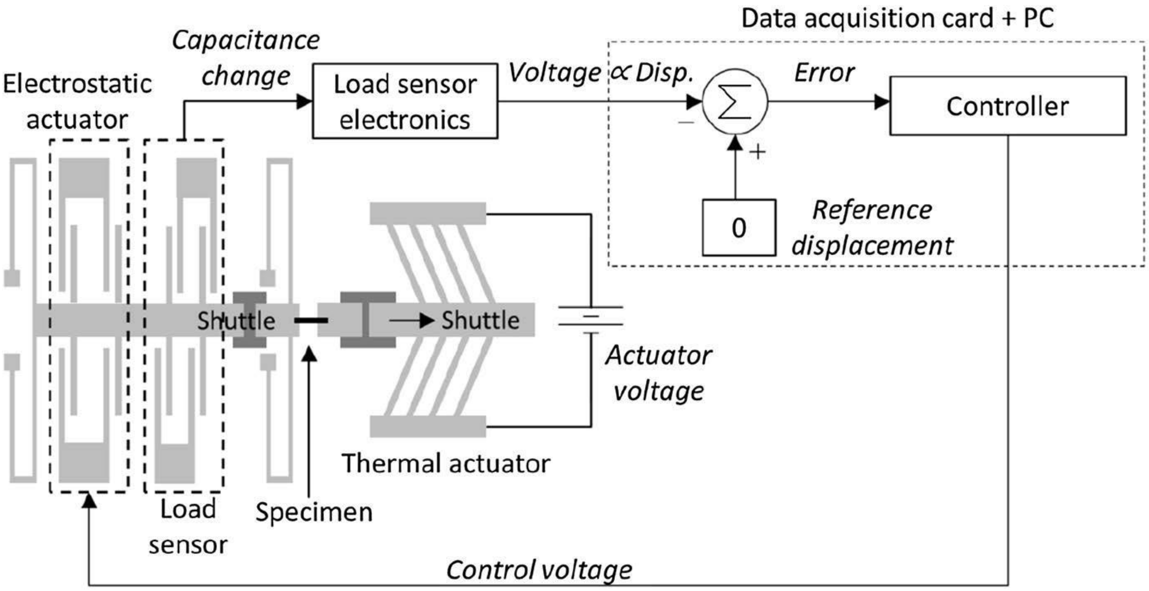

Figure 1.26: A schematic of the closed-loop system for load beams [39].

S. Gupta and O. N Pierron [40] developed a small size 1 mm by 3 mm MEMS device which is small enough to fit inside the electrical biasing holder and can easily place inside the TEM and is fabricated by the SOIMUMPS.

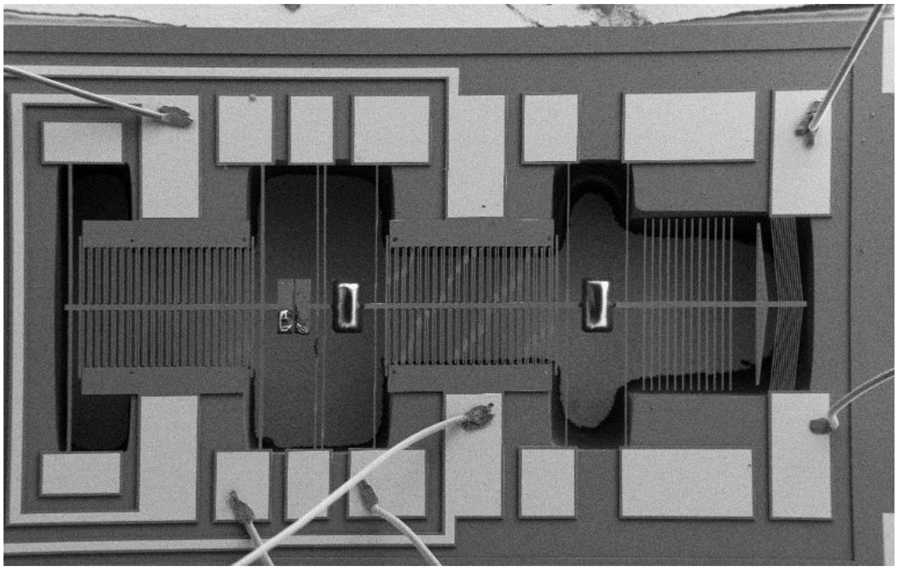

Figure 1.27: A SEM image of the wired board device [40].

It consists of an integrated electrothermal actuator of silicon along with two capacitive sensors one for the displacement measurement and the other for the load measurement with attached beams. They used 4V with a step of 0.25V which is very large and due to this a large amount of heat is generated with large displacement and force. To avoid the heat transfer to the specimen they used large heat sink beams and two air gaps one is in between the actuator and the rest of the device structure and the other is in between the two capacitive sensors. These air gaps are filled with epoxy glue and which also served as isolation between the capacitive sensors and the actuator which prevents the heat transfer from the actuator to the specimen.

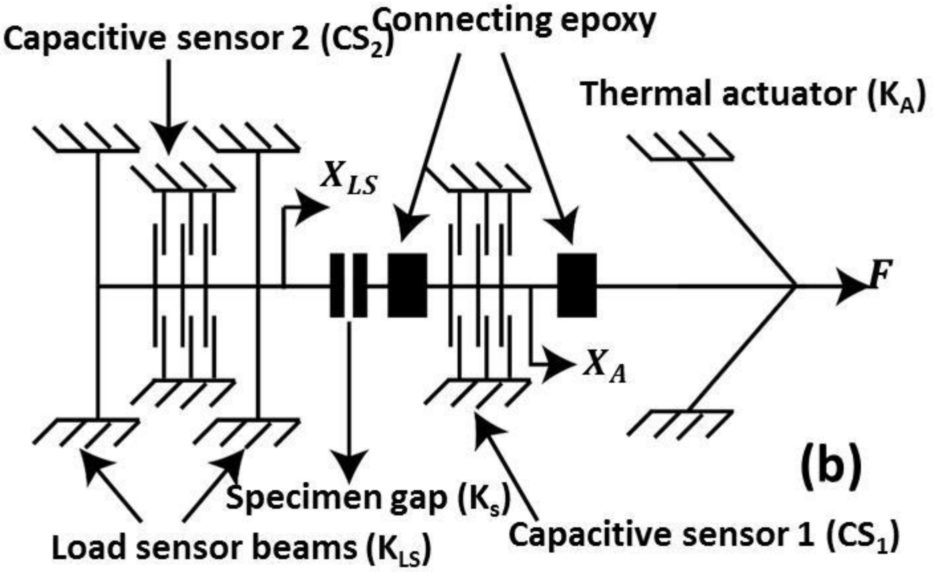

Figure 1.28: A schematic of MEMS devices showing different components [40].

A. M Beese et al. [41] used the same testing system as used by H. D. Espinosa et al. [19] with some modifications in the heat sink beams and the gap between the shuttle for the specimen. They used it to test the nanofibers having diameters ranging from 100 nm to 3nm.

T. Tusachiya et al. [42] revised their design presented in the [36] to test the nanofibers. They change the electrostatic comb drive actuator from interdigitated to parallel plate comb drive to get the small force with a higher resolution to test the nanofibers more reliably.

C. Haward et al. [43] used a novel techniques with consumable test structures available commercially by a company in the market. They tested a high dose of Inconel X-750 and draw its stress-strain graph. The specimen is fixed between the gap of 2.5 μm and a punch is used to push the upper part of the test structure by which the lower part of the structure pushes down and applies a pulling force on the specimen. Bending beams are designed as moveable parts of the test structure which are deflected under the loading phenomenon. The digital image correlation software developed in *Python* known as Shift is used for the continuous point by point tracking of the specimen mark. By using a technique of matching the time of the video and the load-displacement text file they draw a stress-strain curve of Inconel X-750. This technique can be used to test the different specimens without any temperature gradient which leaves errors in the results.

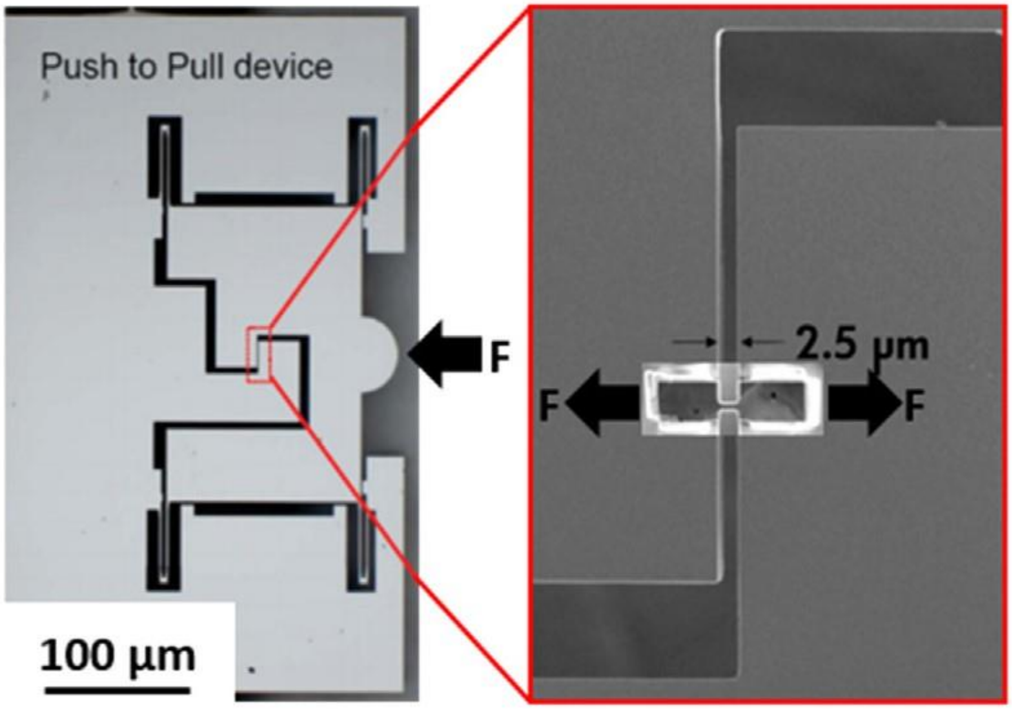

Figure 1.29: The push-pull schematic of MEMS devices [43].

C. Li et al. [43] used novel MEMS devices for tensile testing of the different material nanowires with a comb drive actuator which can produce constant load without any heat generation. The device consists of a comb drive electrostatic actuator and two capacitive sensors. One for displacement measurement and the other for the load measurement with an O-shaped load cell consisting of four clamped guided beams and a gap for the specimen mounting. The specimen is mounted in the gap and load is applied by the comb drive electrostatic actuator at a constant rate. The specimen deformed O-shaped load cell change is shaped according to the applied load. There is no need for any external imaging source for the measurement of the stress and the strain as used in most of the material testing techniques.

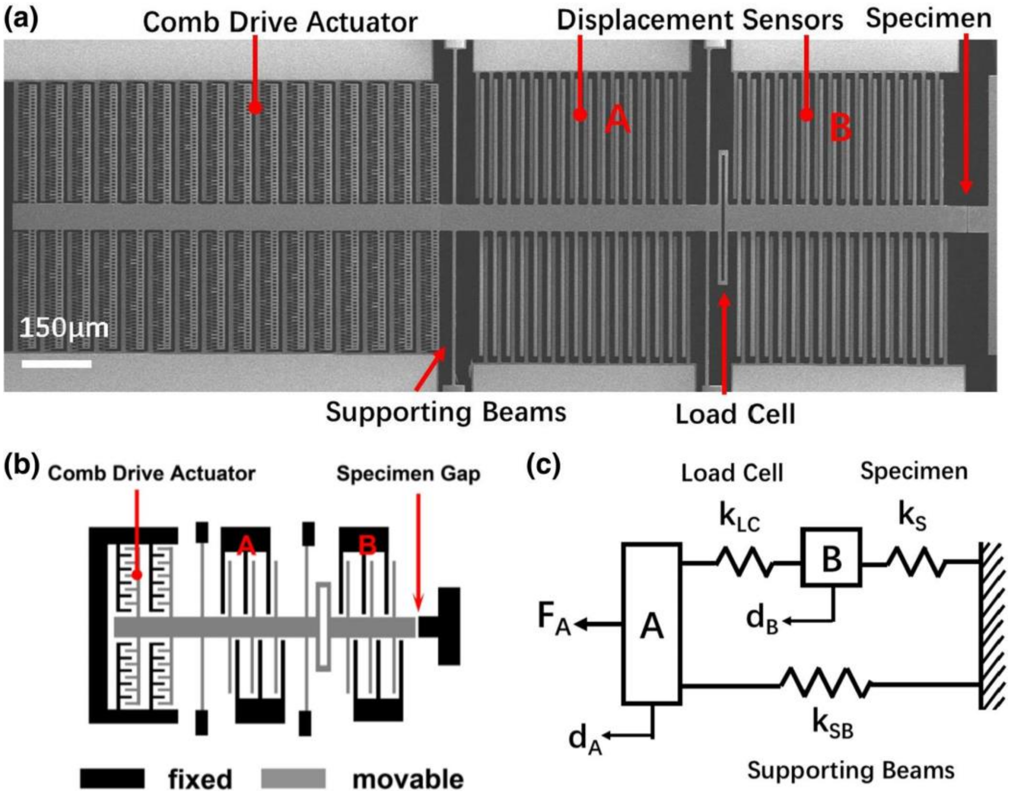

Figure 1.30: (a) MEMS devices image from the SEM (b) Schematic of the device (c) Lump mechanical modal of the device during the test [43].

Chapter 2: Design of MEMS Tensile Testing Machine

The designing of a MEMS-based universal testing machine to find the yield stress of different materials at the micron and the submicron level we need an actuation system to apply the load to the specimen and a sensor that can measure the deflection and the applied load. First, we will analyze different actuation methods that are used at the MEMS level the force application, and then we will select a suitable one for our design. Table 2.1 shows a comparison between different types of actuation methods.

Table 1.1: Comparison of different actuation techniques at the MEMS level.

Specification	**Electromagnetic**	**Piezoelectric**	**Electrostatic**	**Electrothermal**
Deflection	Large	Small	Medium	Large
Input Power	High	Medium	Low	Very High
Operating Speed	Moderate	Fast	Moderate	Slow
Fabrication Process	Complex	Need Exotic Material	Relatively Complex	Simpler
Foot Print	Large	Small	Large	Medium

We need a simple actuation process for the ease fabrication process and need large actuation force and displacement that is why we select an electrothermal actuator for the proposed designs. Further, there are two types of electrothermal actuators Z-shaped and V-shaped.

From a detailed comparison of V and Z shaped actuators by Z. Zhang et al. [44] it's clear that the V-shaped actuator is more suitable for our design due to its superior properties over Z-shaped actuators like large force and displacement.

In the V-shaped actuator, we have different types of material options like single-crystalline silicon, polycrystalline silicon, gold, and nickel, etc. But we select Nickel as material due to its higher coefficient of thermal expansion as compared to the single crystalline silicon and polycrystalline silicon and higher melting point as compared to gold. But it has one drawback that its melting point is far less than the single-crystalline silicon and polycrystalline silicon which limit its usage. In our case, we are also trying to keep the operating temperature as low as possible to avoid the heat transfer to the specimen which can cause different types of errors due to the change of the material properties and to keep it lower than the softening temperature. The material properties of the nickel are given in table 2.2.

Table 2.2: Material properties of nickel [45].

Properties	**Values**	**Units**
Resistivity	20×10^{-8}	Ωm
Conductivity(Thermal)	91	$W.m^{-1}.K^{-1}$
Elastic Modulus	214×10^{9}	$N.m^{-2}$
Thermal Coefficient of Expansion	1.27×10^{-5}	K^{-1}
Density	8908	$Kg.m^{-3}$
Poisson's Ratio	0.3	-
Yield Strength	120	MPa

We have used nickel as a material for the actuator design that's why we will use the MetalMUMPS fabrication process. With this, we will fabricate the actuator along with the rest of the structure in a single layer deposition of 20 µm thick with a minimum gap of 2 µm. Secondly, we need a sensor with a high resolution in the range of submicron levels to measure the deformation in the specimen. The differential capacitive comb drive sensors are the best option for this.

2.1 Proposed Designs for Testing Machine

We proposed two different designs to investigate the yield stress of different materials at micron and submicron levels. The first design is for biaxial tensile testing depicted in figure 2.1 and the second on for uniaxial tensile testing in figure 2.2. Both are made of nickel material by the MetalMUMPS fabrication process.

2.1.1 Biaxial Tensile Testing Machine

The proposed design for biaxial tensile testing is machine is depicted in figure 2.1

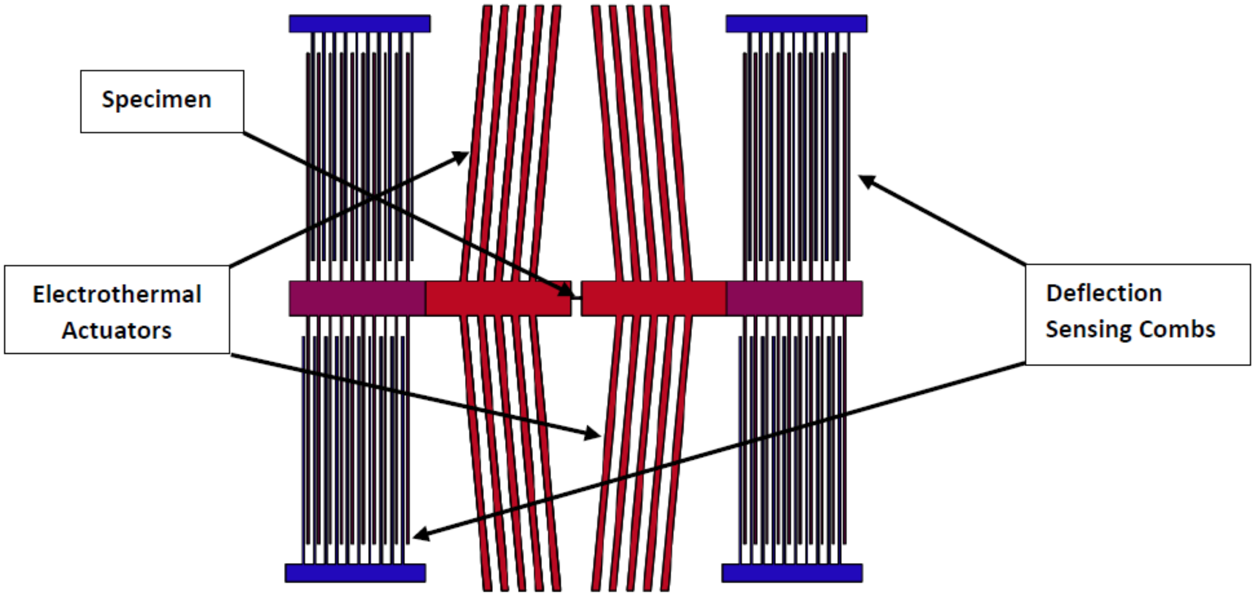

Figure 2.1: Schematic of the MEMS Biaxial Testing Machine.

The biaxial tensile testing machine consists of two chevron type electrothermal actuators of the same configuration with the two identical differential combs drive attached at their ends. A specimen is glued in between these two actuators and when the same voltage is applied to the actuators at the same time they generate equal forces in the opposite direction which try to pull apart the specimen. In the elastic region, a smooth change in the capacitance is observed and when the stress reached the yield point of the specimen material. The strain enters from the elastic to the plastic region and at this point deflection in the comb drives is no more smooth and an abrupt change is observed at this point which is recorded with the help of the supporting electronic circuit. Corresponding stress to that point is known as yield stress of the material. The system is designed for a variety of sizes and materials.

2.1.2 Uniaxial Tensile Testing Machine

The uniaxial tensile testing machine to measure the yield strength of different materials is depicted in figure 2.2.

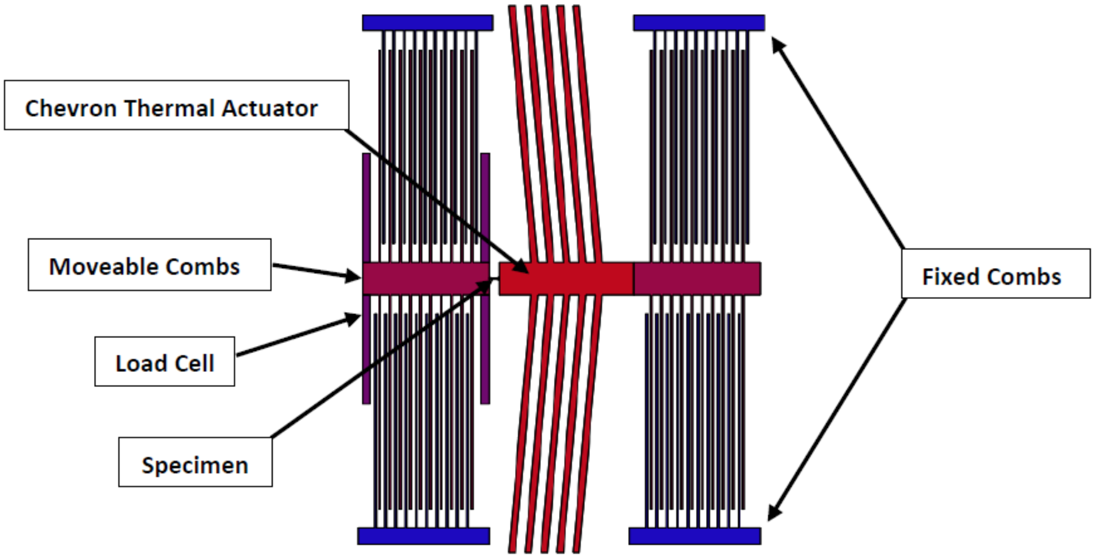

Figure 2.2: Schematic of the MEMS Uniaxial Testing Machine.

The uniaxial tensile testing machine having one chevron type electrothermal actuator directly attached to the deflection sensing differential capacitive comb drive from one end and to the specimen from the other end which is next attached to the load cell in figure 2.2. The load cell consists of a differential capacitive comb drive with load cell beams design to produce a desire deflection at different applied loads.

When the voltage is applied to the actuator it tries to pull the specimen and load cell show deflection which is directly proportional to the applied load and the deflection comb drive gives the overall deflection in the system which is equal to the sum of the load cell deflection and the specimen elongation. Thus we can measure the applied load and the corresponding strain in the specimen at any point.

Now we will design the suitable modal for the chevron type electrothermal actuator, the differential capacitive comb drives, and the deflection beams of the load cell with the help of their mathematical models.

There are two types of electrothermal actuators on the base material single material [46] and another bimorph [47] for out of plan actuation. As we need to in plan actuation so use single material actuator

2.2 Mathematical Model of Chevron Type Electrothermal Actuator

The mathematical modeling of the ETA used in the actuation of the proposed tensile testing machines is presented in this section. The proposed model of the chevron-shaped electrothermal actuator is further divided into two sub-models. The electro-thermal sub-model to predicting the temperature rise in the chevron-shaped beams by application of the input voltage, and the thermal-mechanical sub-model for calculating the maximum output displacement along with force generation by the chevron-shaped actuator. Based on the combination of these two sub-models, a complete system model is developed. Both for the air and the vacuum condition are considered in the proposed electro-thermal sub-model. Additionally, the impacts of the shuttle and the number of beam pairs are also taken into account for increasing design space and flexibility.

The schematic of the chevron-shaped electrothermal actuator is depicted in figure 2.3.

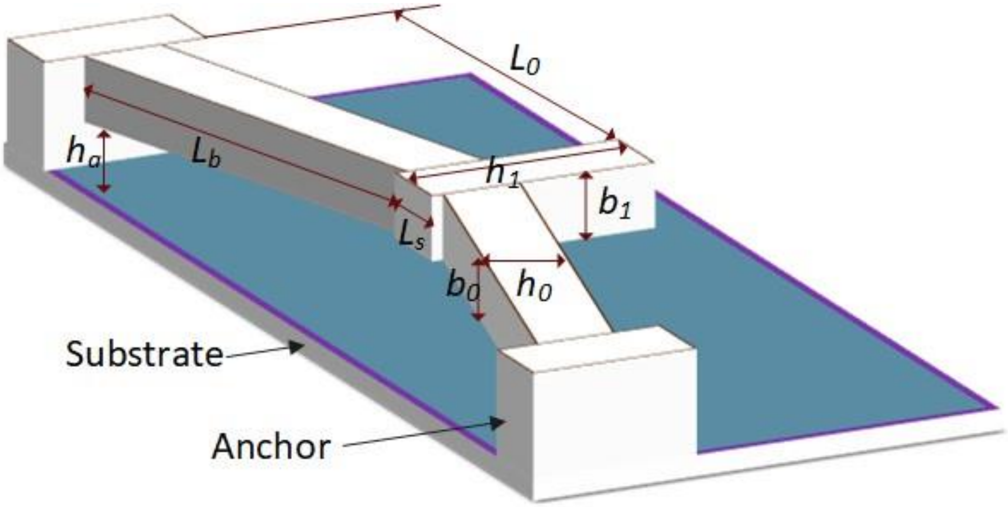

Figure 2.3: Schematic of the chevron-shaped electrothermal actuator [48].

Where the air gap between the structure and the substrate is denoted by ha, distance between the shuttle and the anchor point by L_0 while the beam length is denoted L_b (i.e. for a V-shaped beam, $L_b = L_0 cos\theta$). When the voltage V is applied to the beam anchors, heat is generated due to Joule heating, and the beam will expand symmetrically pushing the central shuttle in the forward direction. The lifetime of an ETA is greatly affected by the operational temperature, and therefore the actuators are expected to operate in lower temperatures. This makes the model using constant-value material properties reasonable and useful as in lower temperatures the influences of the temperatures on the material properties are small so these can be neglected. The influences of temperature change on each material property will cancel out to a certain degree, making the simple closed-form model more accurate than expected.

2.2.1 Electro-thermal modeling

The electro-thermal modeling of the chevron type electrothermal actuators for v-shaped beams is discussed here in this section. The radiation and heat convection effects are so small to be neglected without significantly compromised in the output response of the system for both ambient and vacuum conditions. To keep the model simple, the common working conditions i.e. in air and vacuum are discussed without including the effects of varying ambient pressure on convection and radiation. Heat conduction in this model is considered to be the dominant heat transfer mechanism. One-dimensional (1D) heat conduction is assumed for this model due to the geometrically thin and willowy shape of the beams. The length dx of the differential element in the governing electro-thermal equation is given as [49].

$$k\frac{d^2T}{dx^2} - \frac{k_a(T - T_0)}{bh_a} + \dot{q} = 0 \tag{2.1}$$

Where k represents the thermal conductivity of beam, k_a is the thermal conductivity of the air and T_0 is the room temperature. The first term on the left illustrates the heat conduction of the structure (i.e. shuttle and the beams). The second term describes the air gap which is equal to zero for vacuum conditions. The third term is the heat source term which is calculated for beam and shuttle respectively can be written as

$$\dot{q_b} = \frac{A_s^2}{\hat{\rho}(2L_bA_s + nL_sA_b)^2}V^2 \tag{2.2}$$

$$\dot{q_s} = \frac{n^2A_b^2}{\hat{\rho}(2L_bA_s + nL_sA_b)^2}V^2 \tag{2.3}$$

where $\hat{\rho}$ is electrical resistivity of the structure, n is the number of beam pairs,L_s and L_b are shuttle and beam lengths respectively and the cross-sectional areas of the shuttle and beam are represented by A_s and A_b respectively. The governing equation 2.1 is solved while considering the boundary conditions as follows:

(1) The temperature at anchors and the substrate is at room temperature T_o during the whole operation of the device.

(2) The temperature of the shuttle and beams should be the same at $x = L_b$ and $x = L_b + L_s$.

(3) The rates of heat conduction should also be the same at $x = L_b$ and $x = L_b + L_s$

Solving equation 2.1 by using the boundary conditions, the average temperature increase of the beams for both vacuum and ambient conditions can be expressed in a general form as shown in equation 2.4. It is clear that the average temperature rise along the beams ΔT_{b_avg} is dependent on material properties represented by$Q$, the structure of beams represented by T, and input voltage represented by V.

$$\Delta T_{b\_avg} = Q.T.V^2 \tag{2.4}$$

Whereas for 'in vacuum' case,

$$Q = \frac{1}{12k\hat{\rho}} \tag{2.5}$$

$$T = \frac{A_s L_b (4A_s L_b + 3nA_b L_s)}{(2L_b A_s + nL_s A_b)^2} \tag{2.6}$$

and for 'in air' case,

$$Q = \frac{1}{k_a \hat{\rho}} \tag{2.7}$$

$$T = \frac{(1 - s_1)^2}{L_b r_1 s_1} O_1 + (\frac{1 - s_1}{L_b r_1 s_1}) J_1 \tag{2.8}$$

And

$$A_s = h_1 b_1 \tag{2.9}$$

$$A_b = h_0 b_0 \tag{2.10}$$

$$s_1 = e^{L_b r_1} \tag{2.11}$$

$$r_1 = \sqrt{{k_a}/{k b_0 h_a}} \tag{2.12}$$

$$J_1 = \frac{A_s^2 b_0 h_a}{(2L_b A_s + nL_s A_b)^2} \tag{2.13}$$

$$O_1 = \frac{s_1(J_2 - J_1) + J_1}{s_1^2 - 1} + \frac{n(n_4 + 1)s_1[A_b r_1 (s_1^2 + 1)(J_1 - J_2) - 2A_b r_1 s_1 J_1]}{(s_1^2 - 1)[A_s R_2 (1 - s_4)(s_1^2 - 1) + nA_b r_1 (s_4 + 1)(s_1^2 + 1)]} \tag{2.14}$$

$$s_4 = e^{-L_s R_2} \tag{2.15}$$

$$R_2 = -\sqrt{{k_a}/{k b_1 h_a}} \tag{2.16}$$

$$J_2 = \frac{n^2 A_b^2 b_1 h_a}{(2L_b A_s + nL_s A_b)^2} \tag{2.17}$$

2.2.2 Thermo-mechanical Modeling

The pushing of the shuttle in the forward direction is caused by the symmetrical thermal expansion of beams. The output displacement can be calculated using the Castiglione's theorem while assuming the deformation of the beams to be linear [44, 49].

On the V-shaped beam, the applied bending moment M is given by,

$$M = Fx\sin\theta - Px\cos\theta - M_1 \tag{2.18}$$

Where P is the external force

The axial force is applied on the beam is given by $N = F\cos\theta - P\sin\theta$. The tip displacement of the beam is given as

$$y_{max} = \Delta L_T \sin\theta - \int_0^{L_b} \frac{N}{EA_b}\frac{\partial N}{\partial P}dx - \int_0^{L_b} \frac{M}{EA_b}\frac{\partial M}{\partial P}dx \tag{2.19}$$

Where Young's modulus of beam material is represented by E and the axial elongation of the beam caused by thermal expansion is represented by ΔL_T. ΔL_T can be calculated as $\Delta L_T = \alpha(\Delta T_{b\_avg})L_b$, where α represents the thermal expansion coefficient. Assuming the following boundary conditions

$$\delta_{\theta_c} = \int_0^{L_b} \frac{M}{EI}\frac{\partial M}{\partial M_1}dx = 0 \tag{2.20}$$

$$\Delta L_T \cos\theta - \int_0^{L_b} \frac{N}{EA_b}\frac{\partial N}{\partial F}dx - \int_0^{L_b} \frac{M}{EI}\frac{\partial M}{\partial F}dx = 0 \tag{2.21}$$

Equation 2.48 can be solved for tip displacement as follows

$$y_{max} = \begin{pmatrix} \alpha B_1 & 0 \\ 0 & -\dfrac{1}{2nE}B_2 \end{pmatrix} \begin{pmatrix} \Delta T_{b\_avg} \\ P \end{pmatrix} \tag{2.22}$$

where for V-shaped beam:

$$B_1 = L_b B \sin\theta \tag{2.23}$$

$$B_2 = {}^{BL_b}\!/_{A_b} \tag{2.24}$$

$$B = {}^{L_0^2}\!/_{(h_0^2 \cos\theta^4 + L_0^2 \sin\theta^2)} \tag{2.25}$$

It is clear from equation2.51 that the output displacement is reliant on the temperature increase along the beams (ΔT_{b_avg}), the external load (P), material properties (α and E), and structure of beams (B_1 and B_2).

2.2.3 System Modeling

The system model for output displacement can be written in compact form by merging the electro-thermal and thermal-mechanical models as[50].

$$y_{max} = (F_1 - F_2)\begin{pmatrix} V^2 \\ P \end{pmatrix} \tag{2.26}$$

Where

$$F_1 = \alpha Q B_1 T \tag{2.29}$$

And

$$F_2 = {}^{B_2}/_{(2nE)} \tag{2.30}$$

Here, F_1 is the flexibility due to applied voltage V and F_2 is the flexibility of the thermal actuator owing to external force P with the resultant stiffness's of $K_1 = {}^{1}/_{F_1}$ and $K_2 = {}^{1}/_{F_2}$ respectively. In aspects of generating force and tip displacement, the input voltage and external forces are comparable. Equation 2.31 can be rewritten as

$$y_{max} = F_2 . F_{max} = F_2 . (P_V - P) \tag{2.31}$$

here $P_V = ({}^{F_1}/_{F_2})V^2$represents the force corresponding to the applied voltage on the actuator. F_{max} is defined as the output force of the actuator of stiffness K_2 at the maximum displacement y_{max} and is given by

$$F_{max} = (P_V - P) \tag{2.32}$$

Let $\eta = {}^{F_1}/_{F_2}$, then the output force can be rewritten as

$$F_{max} = \eta V^2 - P \tag{2.33}$$

The effects of the input factors (i.e. applied voltages and loads), physical parameters (shuttle and beam geometry), and material-dependent properties (i.e. resistivity and Young's Modulus) on the outcomes (i.e. displacement and output force generation) can be observed with the help of this linear closed-form system model, which greatly facilitates the design analysis of the thermal actuators.

By setting the thermal conductivity of air k_a close to zero or by assuming a sufficiently large air gap, the model for the 'in air' case simply reduces to the model for the 'in vacuum' conditions.

The stiffness-force model of V-shaped electro-thermal actuator indicates that maximum displacement and output force generated is directly related to the chevron stiffness K_{chev} which is dependent on the inclination angleθ. Variation in stiffness, output displacement, and force generation can be achieved by changing the values of the inclination angle.

2.3 Mathematical Modeling for Load Sensor Beam

The load cell consists of four fixed guided beams and a differential capacitive comb drive. The fixed guided beams are in the parallel arrangement so the spring constant of the load cell is equal to the sum of their spring constants *4k*. Where *k* is the spring constant of a single fixed guided beam. The spring constant of the fixed guided beam [4].

$$k = \frac{E \times w \times t^3}{4 \times l^3} \tag{2.34}$$

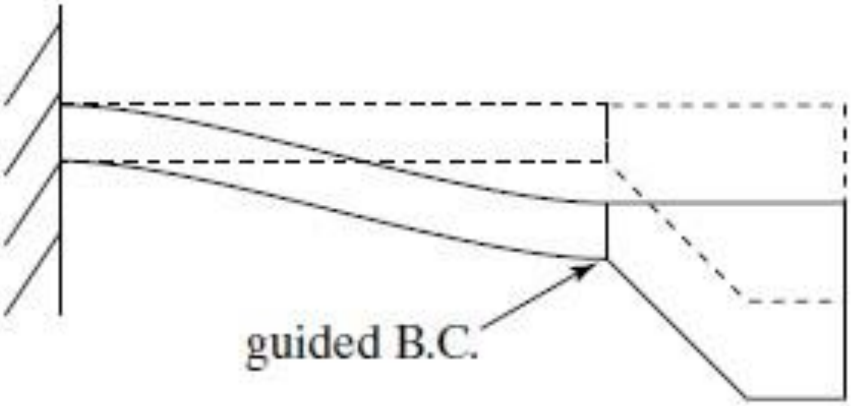

Figure 2.4: Schematic of the fixed guided beam [4].

Where E the young's modulus of the beam material, w is the width of the beam perpendicular to the applied load, t is the thickness of the beam parallel to the applied load and l is the length of the beam to adjust the deflection of the beams we used Hook's law according to the applied load.

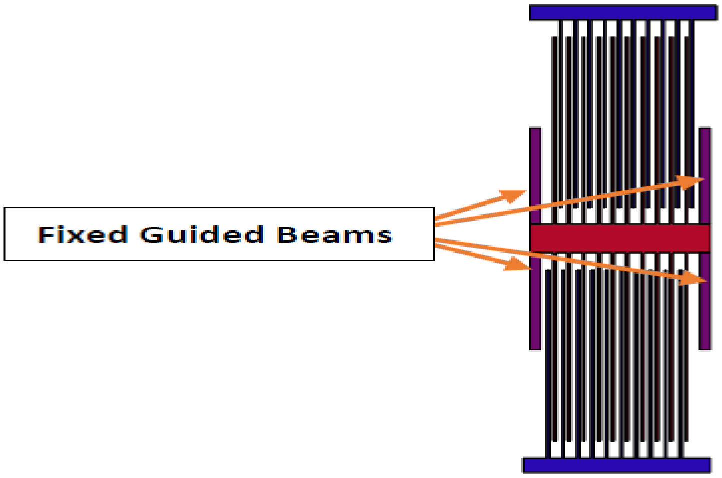

Figure 2.5: Schematic of the proposed load cell.

$$F = 4k \times x \tag{2.35}$$

Where x is the desired deflection of the beam at a given load. We set this 1 µm in our case. As we are, testing the Gold and Nickel specimens having yield strengths 120 MPa and 400 MPa respectively.

The specimen dimensions are width 2 µm, thickness 5µm and the length is 10 µm so the area is 10 µm². The applied force at yield the stress according to Hook's law is given by.

$$F = \sigma \times A \tag{2.36}$$

Then the spring constant by equation 2.35 is 1000 Nm^{-1} by using this value we calculate the length of the single fixed guided beam from equation 2.34 which is 195 µm for each beam.

2.4 Mathematical Modeling of Differential Capacitive Sensor

Differential comb drive sensors are used for the load cell in the uniaxial testing machine and deflection sensing in both the uniaxial and the biaxial testing machines. It has a very high sensitivity in the range of submicron levels and gives good output capacitance change which can be easily detected. We set the gap and antigay are set 2.5 µm and 7.5 µm respectively to maximize the sensitivity of the device and to meet the feasibility of the fabrication process.

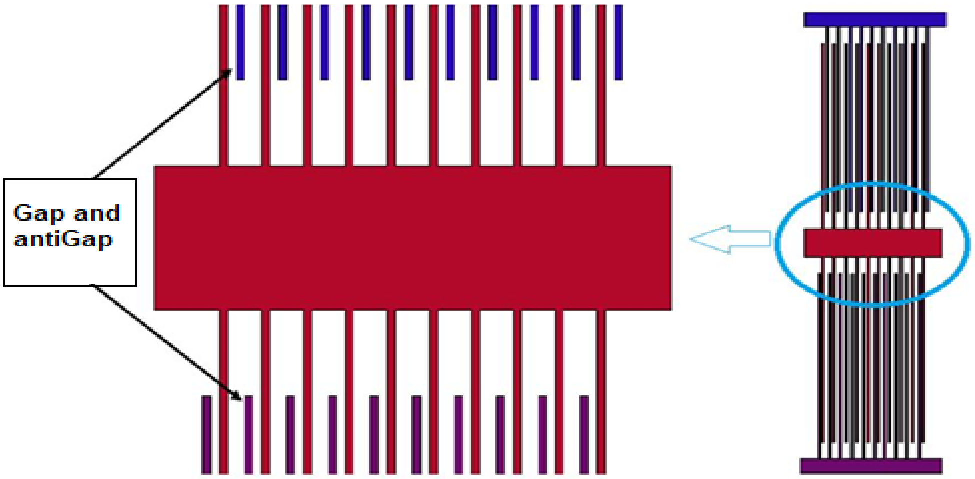

Figure 2.6: Schematic of the differential capacitive sensor with a magnified section.

The change in capacitance and the required numbers of combs for a given geometry can be found by following Equation 2.37 [51].

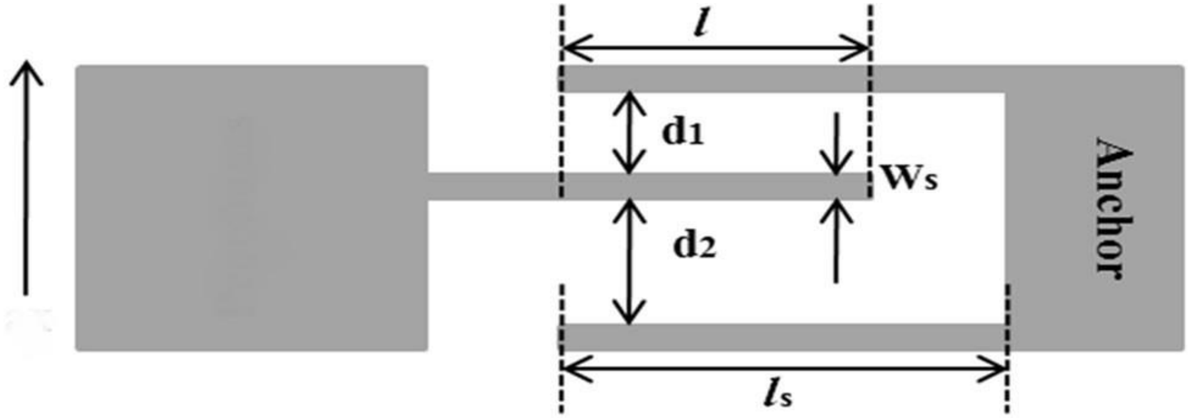

Figure 2.7: Schematic of the differential capacitive sensor [34].

$$N = \frac{\Delta C \times (d1^2 - x^2) \times (d2^2 - x^2)}{2 \times \varepsilon \times l \times t \times (d2^2 - d1^2)} \quad (2.37)$$

Where N is the required numbers of the combs ΔC is changed in the capacitance, $\varepsilon = 8.85\times10^{-12}$ $m^{-3}kg^{-1}s^4A^2$is the permittivity of free space, l is the overlapped length, t is the overlapped thickness and x is the minimum deflection. We set d1 = 2.5µm, d2 = 7.5 µm, ΔC = 180 ft, l = 300 µm, t= 20 µm and x=1 µm. From equation 2.37 the total number of the required comb is 10.

Chapter 3: Finite Element Method Based Modeling

The finite part technique could be a computative technique to manage issues of engineering and mathematical physics. Typical downside areas of interest embrace structural analysis, fluid flow, heat transfer, mass transport, and magnetic attraction potential. FEM based Electro-Thermal and Thermo-Mechanical Analysis.

3.1 FEM based Electro-Thermal and Thermo-Mechanical Analysis

In this Chapter, a comprehensive FEM primarily based simulation methodology is undertaken for both biaxial and uniaxial designs. The FEM could be a numerical technique for getting an approximate answer to the partial differential equations. The small electrothermal mechanism is ruled by these partial differential equations that in result divides the small mechanism domain into a mesh of separate sub-domains known as the finite parts. Then approximate polynomial solutions of those partial differential equations square measure found by these finite parts. Then, to offer a complete answer with an applicable degree of smoothness over the whole small mechanism domain, the approximate polynomial results of every part square measure pieced along. Though absolutely the results of the FEM simulation are subject to approximation errors, sure accuracy will still be achieved with applicable meshing structure.

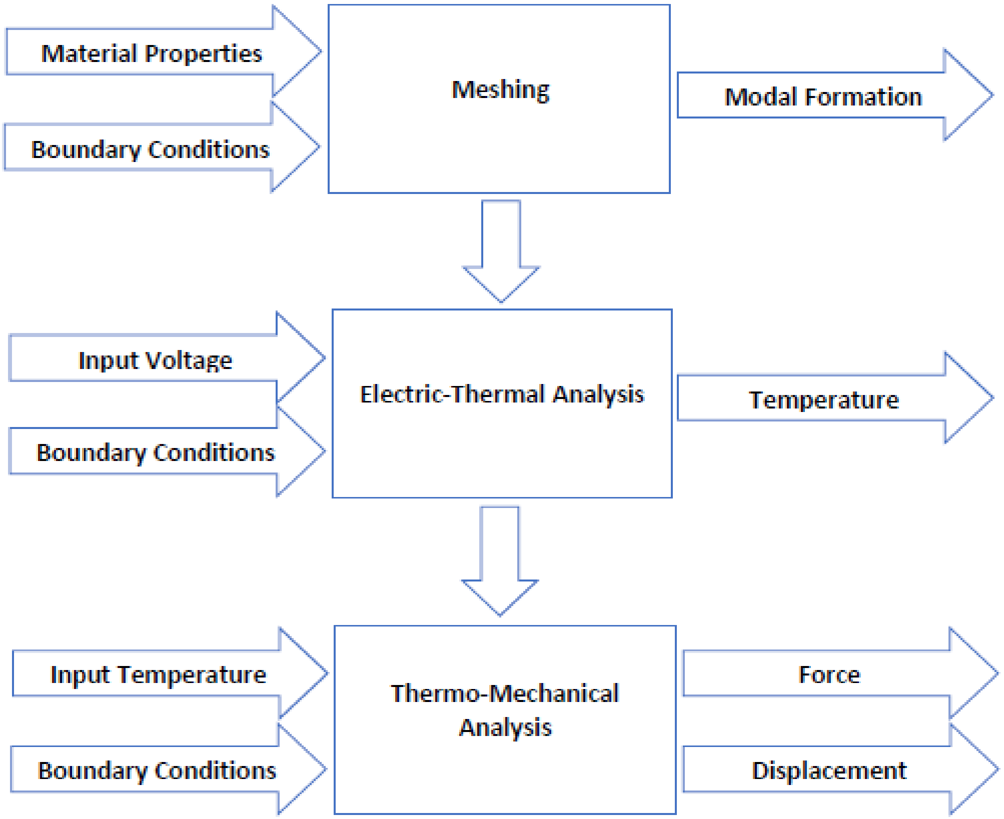

Figure 3.1: The sequential diagram for performing the FEM-based simulations.

The input parameters of the design analysis are shown by the blue arrows in a sequential diagram for performing FEM based simulations whereas the outcomes are shown by the green. To perform these two analyses, we used ANSYS 16.0 workbench, whereas the geometries were made on the Solid works 2017. For the analysis, we selected the analysis systems as follow: -

a) Thermal Electric
b) State Structural Analysis

3.1.1 Electro-Thermal and Thermo-Mechanical Analysis for Actuator

For the electrothermal actuator, an Electrothermal analysis is initially executed to estimate the per degree temperature rise from the ambient on the beams of the ETA & on the specimen for an applied actuation voltage. By increasing actuation voltage there is a noticeable increase in the temperature of electrothermal actuator beams. The maximum temperature for the biaxial testing machine on the hot arms of the electrothermal actuator 39.2 $^\circ C$& is less than 40 $^\circ C$ for the gold specimen for the applied voltage of up to 0.05V. And the maximum temperature on the hot arms of the electrothermal actuator 39.17 $^\circ C$ and 37.17 $^\circ C$ on the nickel specimen at the applied voltage up to 0.05V.

For the uniaxial testing machine, the maximum temperature at the hot arm of the electrothermal actuator is 32 $^\circ C$and less than 32 $^\circ C$ in the case of the gold specimen for the applied voltage of up to 0.05V. And the maximum temperature at the electrothermal actuator is 52.79 $^\circ C$ and less than 40.00 $^\circ C$ at in the case of the nickel specimen at the applied voltage 0.07V.

The temperature profile of the proposed MEMS-based biaxial and uniaxial machines for both gold and nickel are presented in the following figures figure 3.2, figure 3.3, figure 3.4, and figure 3.5.

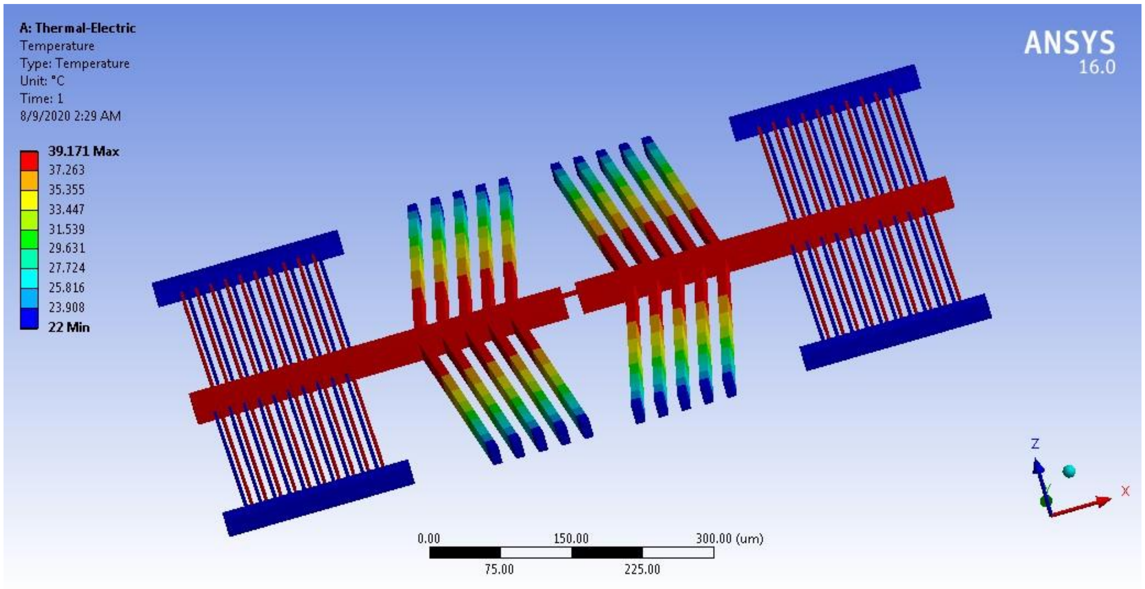

Figure 3.2: Temperature profile for the biaxial machine with the gold specimen for 0.05V.

The plastic strain is achieved at very low applied voltages due to which the temperature rise on the specimens are very low and showed no significant effect on the material properties of the specimens [52].

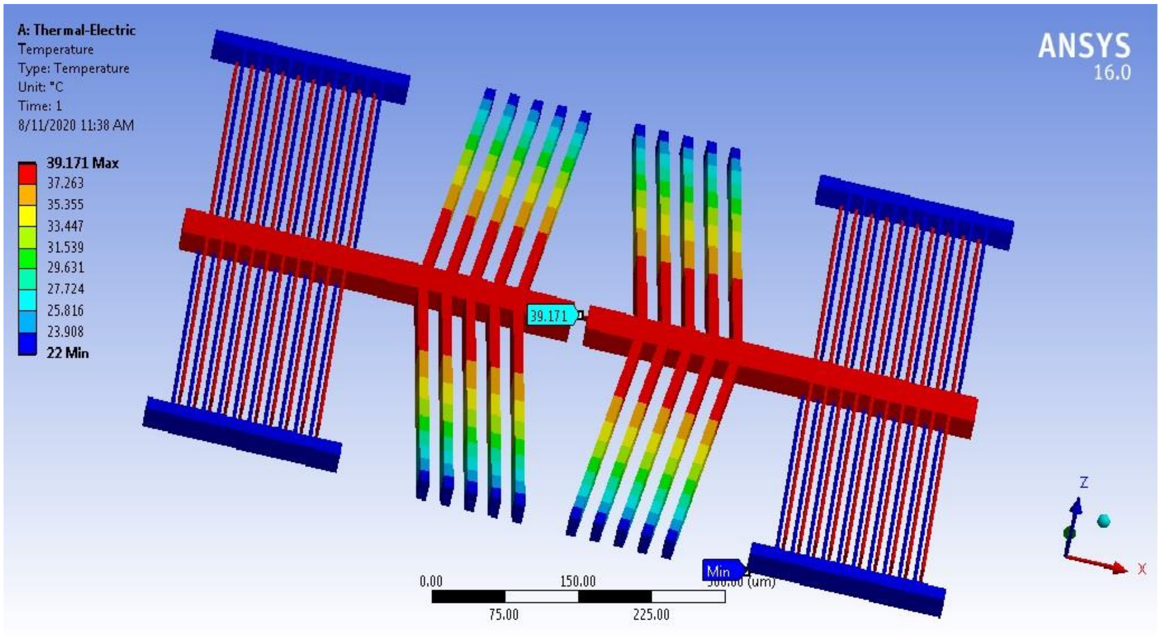

Figure 3.3: Temperature profile for the biaxial machine with the nickel specimen for 0.05V.

For the biaxial tensile testing machine for both the gold and the nickel, specimens' temperature rise are the same due to the same applied voltages.

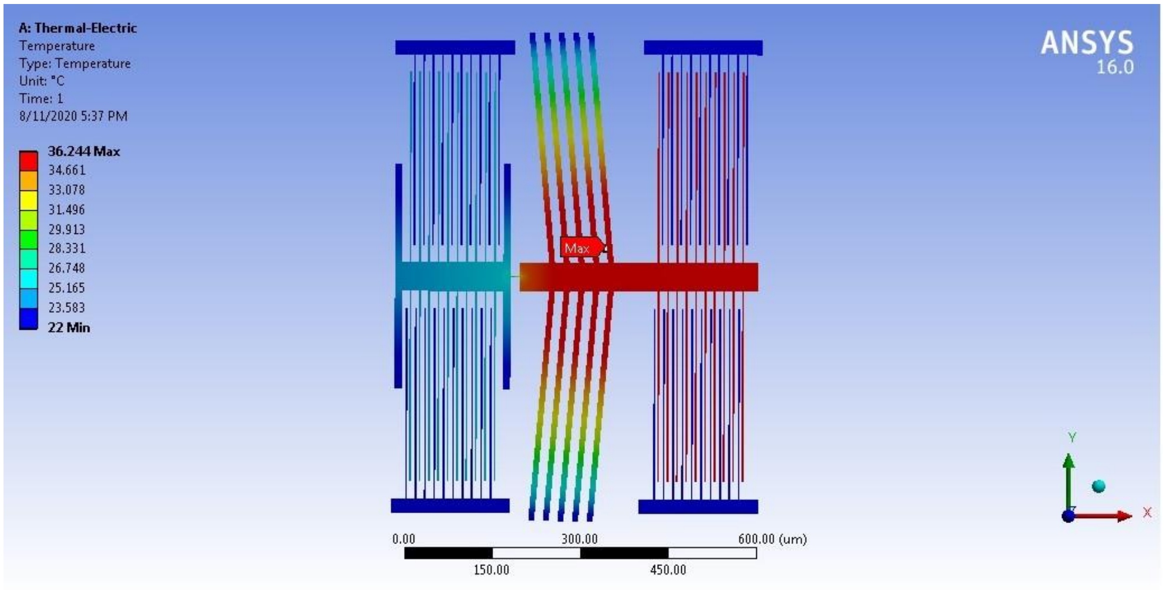

Figure 3.4: Temperature profile for the uniaxial machine with the gold specimen for 0.05V.

The nickel has higher yield strength as compared to the gold that's why we increase the applied voltage to get the yield strength. Due to the increase in the applied voltage the temperature of the ETA and the specimen also increases which can be observed from ANSYS the temperature profile of the nickel specimen in figure 3.5.

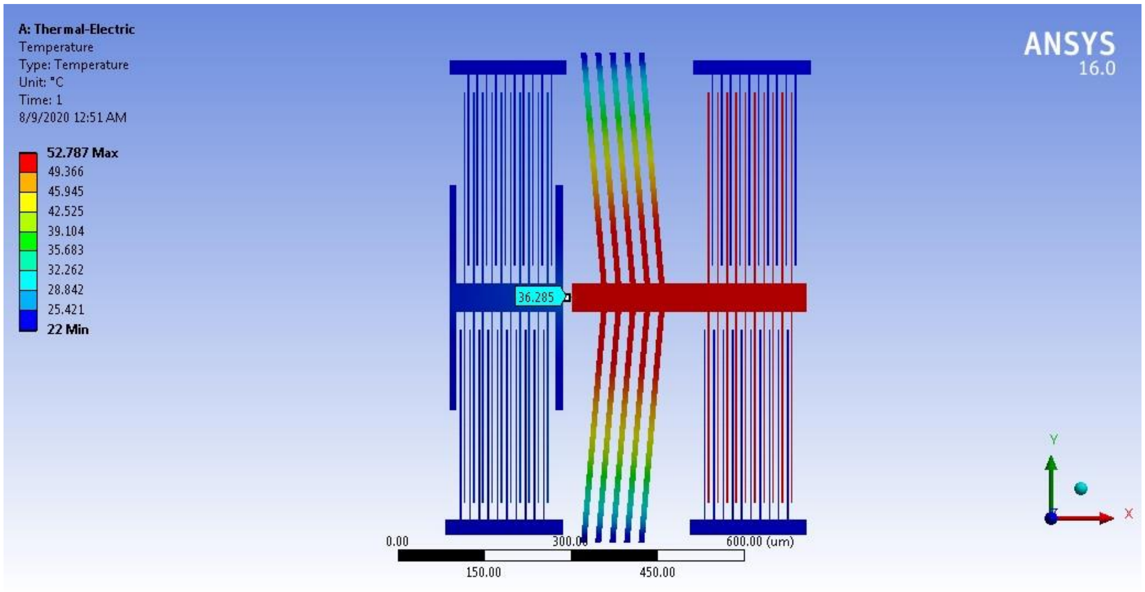

Figure 3.5: Temperature profile for the uniaxial machine with the nickel specimen for 0.07V.

3.1.2 Displacement for Biaxial Tensile Testing Machine

Once the temperature is applied to the thermomechanical system by applying a voltage to the ETA it provides the maximum displacement along the x-axis and small amount out of the plane due to the specimen mounting position in the assembly. A comparison between the gold and the nickel specimen is given in figure 3.6.

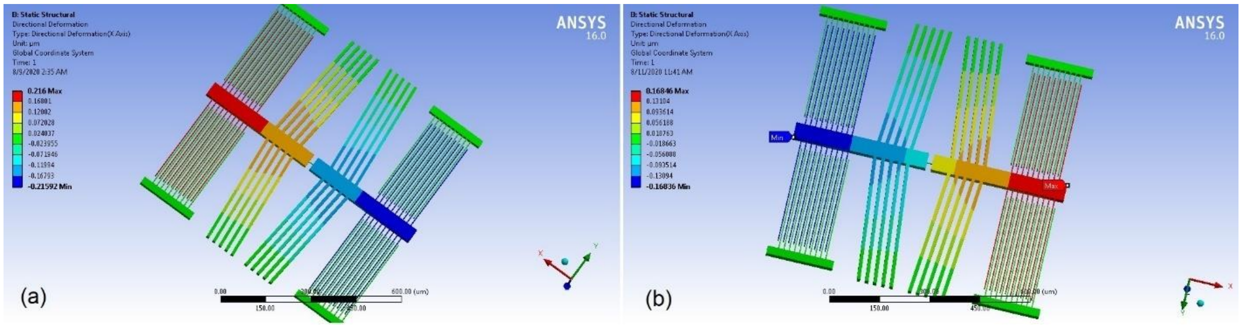

Figure 3.6: Comparison of displacements along the x-axis for the biaxial machine at applied voltage 0.05V (a) the gold specimen (b) the nickel specimen.

A clear difference between the displacements is observed due to the different yield strengths of the gold and the nickel specimens. As the strength of the material increase, the displacement by the ETA decreases for the same applied voltage, and the geometry. It is because the gold specimen has the lower yield strength as compared to the nickel specimen so the displacement is greater because lower stress developed in the specimen and it elongates more as compared to the nickel specimen.

3.1.3 Equivalent Stress (Von-Mises) for Biaxial Tensile Testing Machine

The maximum equivalent stress in the system depends upon the ETA geometry, applied voltage, and the external loading of the system. As the external load increase, the maximum developed stress will also increase and the output displacement will decrease. In the case of the gold specimen having the yield strength 120 MPa the maximum stress developed at the specimen is 495.36 MPa and in the case of the nickel specimen having yield strength 400 MPa the maximum stress developed at the specimen is 597.64 MPa.

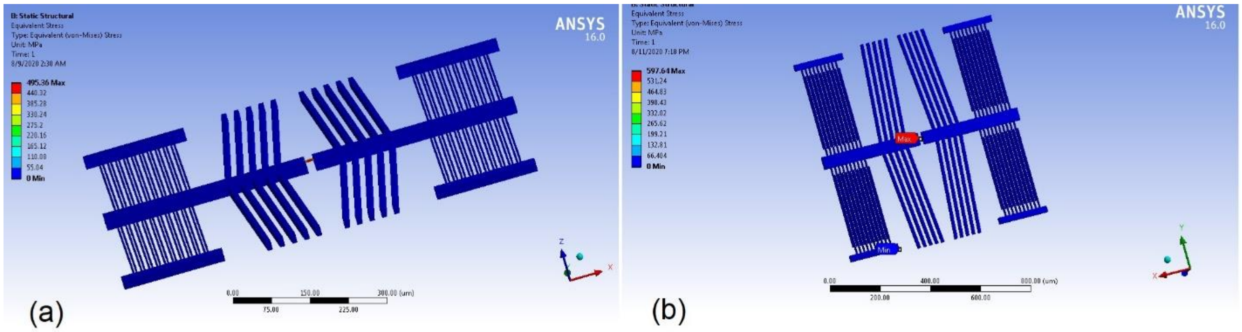

Figure 3.7: Comparison of equivalent (Von-Mises) stresses for the biaxial machine at applied voltage 0.05V (a) the gold specimen (b) the nickel specimen.

The temperature profile in both cases figure 3.6(a) and figure 3.6(b) show that the heat transferred to the specimens is very low without the use of heat sink beams which compromise the applied force [40].

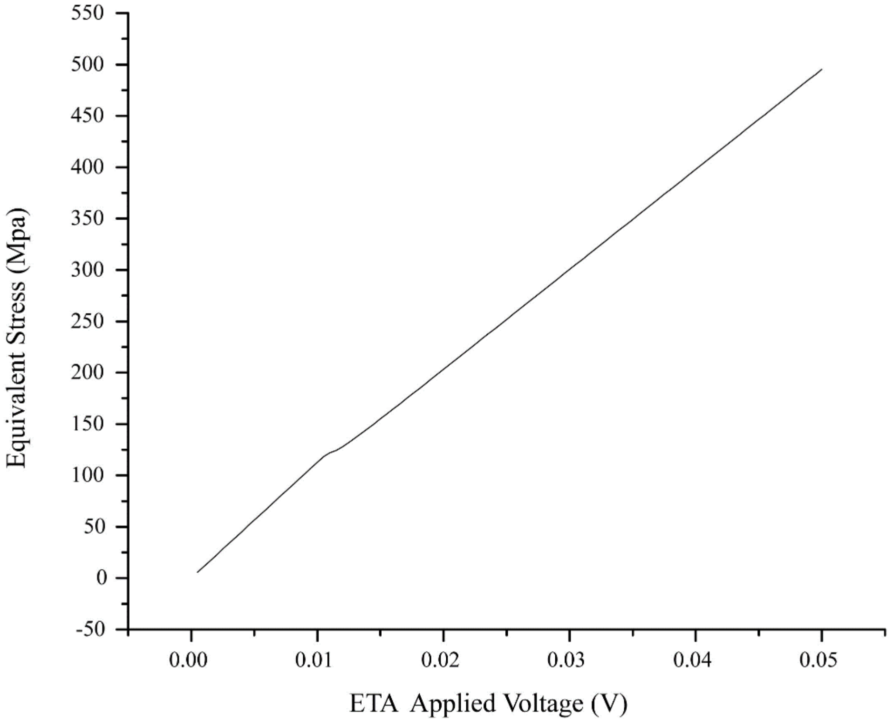

Figure 3.8: Equivalent (Von-Mises) stress versus applied voltage for the gold specimen.

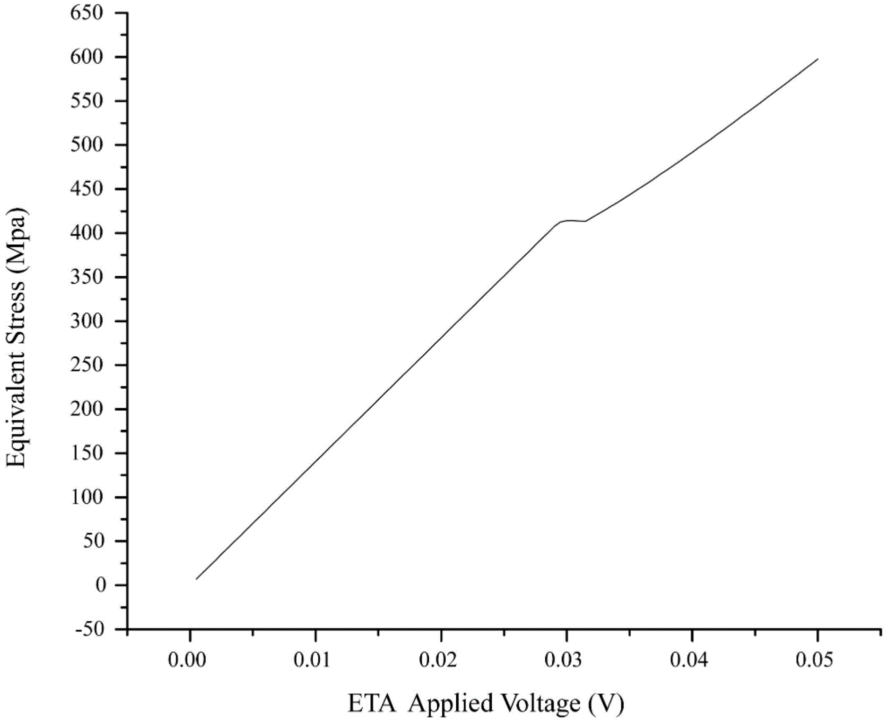

Figure 3.9: Equivalent (Von-Mises) stress versus applied voltage for the nickel specimen.

The graphs show that there is a nonlinear change in the equivalent stress of the system when the yield strength of the specimen is reached and the material enters from the elastic to the plastic region [8].

3.1.4 Equivalent Total Strain (Von-Mises) for Biaxial Tensile Testing Machine

Strain developed in the system when the voltage is applied to the ETA in the elastic region it increases with a constant rate and after the yield point when the material enter from elastic to plastic its slope increase showing that less force is required to deformed the system in this region.

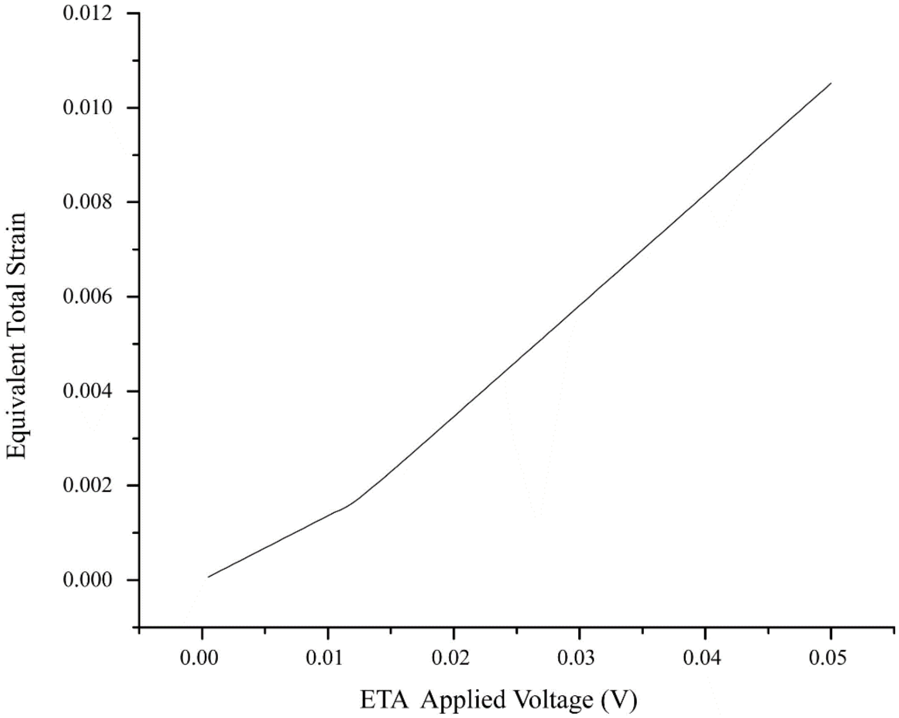

Figure 3.10: Equivalent total strain versus applied voltage for the gold specimen.

The graphs of equivalent total strain against the applied voltage for both for the gold and the nickel specimens show clearly that the strain in the elastic region is low as compared to the plastic region. The material shows more deformation in the elastic region as compared to the plastic in the given range [8].

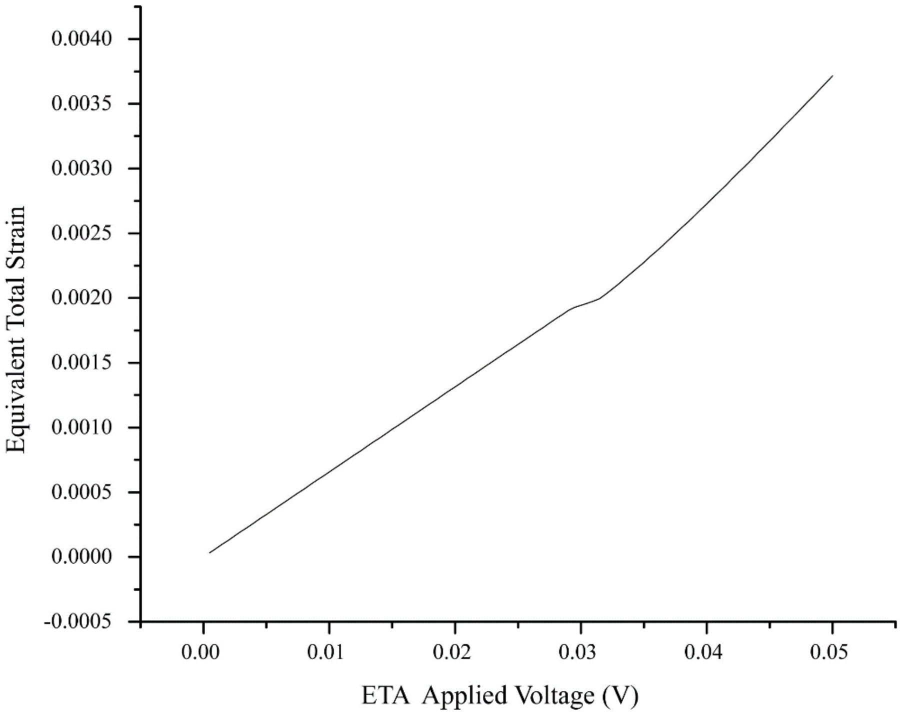

Figure 3.11: Equivalent total strain versus applied voltage the nickel specimen.

3.2 Engineering Graph of Gold and Nickel for Biaxial Tensile Testing Machine

From the FEM analysis values of equivalent stress and total equivalent strain, a graph is drawn to predict the yield stress of the gold and the nickel specimens. The graphs have shown a linear change in the strain against the applied stress up to a certain point after that a nonlinear behavior is developed and the slopes of the graphs changed. The point where this nonlinearity developed is the yield points of the material and the corresponding stress that is known as yield stress of the material. It is clear from figure 3.12 and 3.13 that the yield strengths of the gold and the nickel are 120 MPa and 400 MPa respectively which are the same as the values given in the material properties for the analyses.

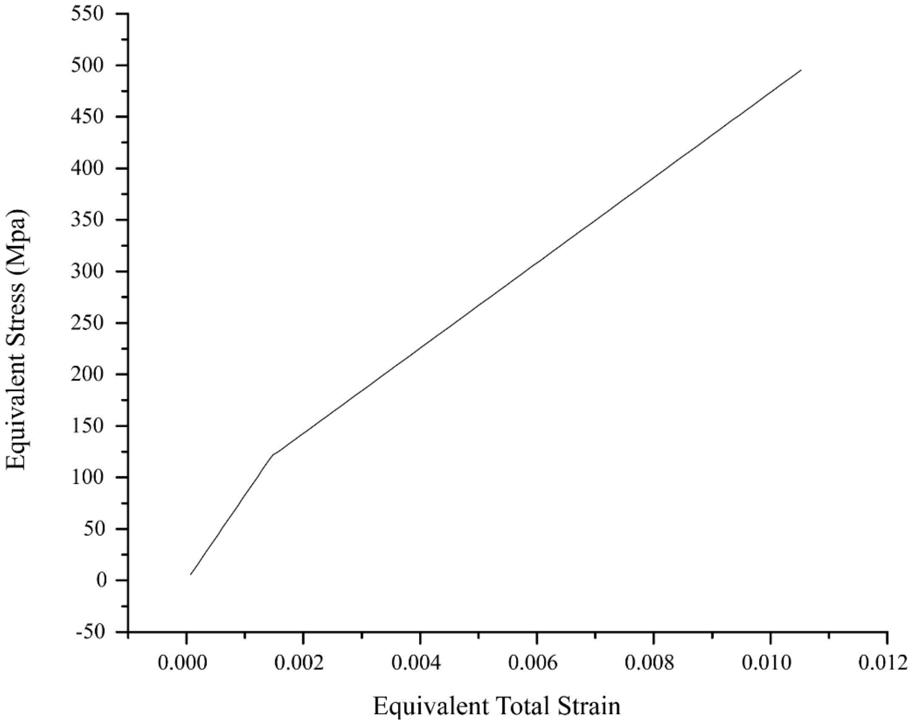

Figure 3.12: Equivalent total stress versus total equivalent strain for the gold specimen.

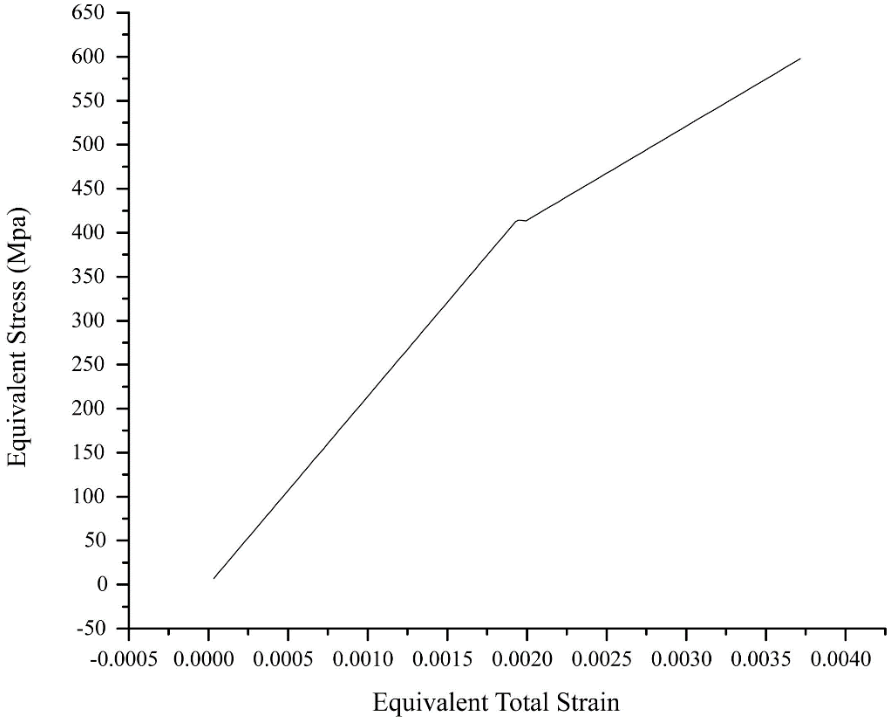

Figure 3.13: Equivalent stress versus equivalent total strain for the nickel specimen.

3.3 FEM Analysis for Uniaxial Tensile Testing Machine

The uniaxial design has one ETA and differential comb drive sensors one for load and another for total displacement sensing. Different voltages are applied to ETA to get the plastic strain in both the nickel and the gold specimens.

3.3.1 Displacement for Uniaxial Tensile Testing Machine

As uniaxial design has two differential comb drives so the displacement is this case is the sum of load cell deflection and deformation in the specimen given by figure 3.14 and figure 3.15 for the gold and the nickel specimen respectively. Actuation voltages 0.05V and 0.07V are used for the testing of gold and nickel specimens respectively to generate a plastic strain in both specimens.

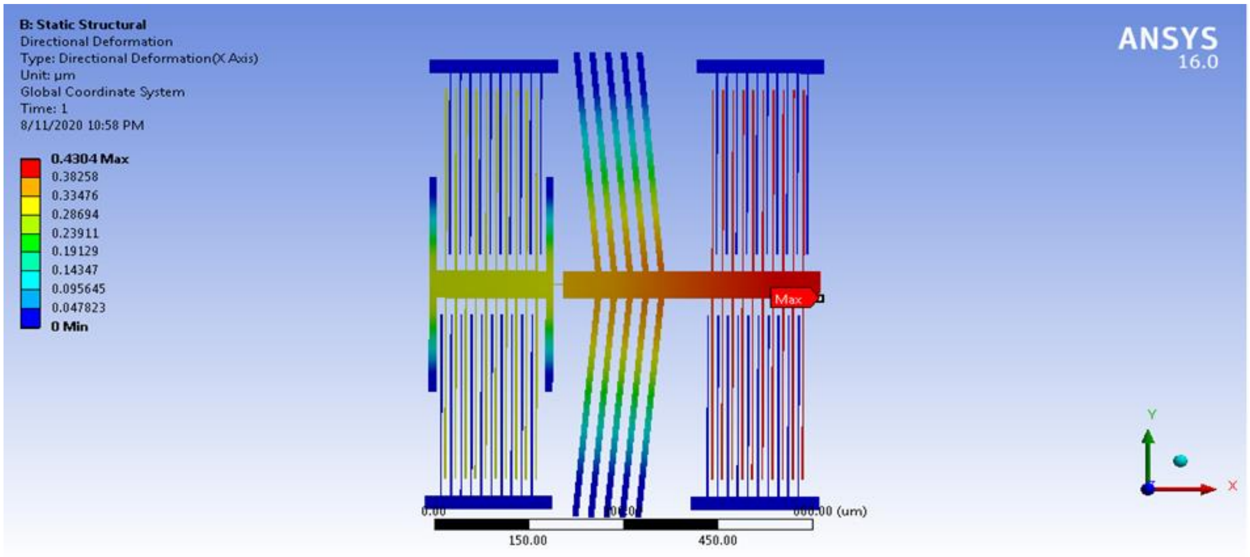

Figure 3.14: Displacements along the x-axis for the uniaxial machine at applied voltage 0.05V (a) the gold specimen.

Figures 3.14 and figure 3.15 show deflection is maximum in displacement sensing comb and minimum at the load cell. When a voltage is applied to the ETA it generates stress in the specimen and corresponding to that stress a deflection is shown in the load cell beams. Due to this deflection, a change in the capacitance is measured with the help of MC3110 [53] or AT1006 [54] to calculate the applied load. These are two commercially available electronic devices for differential readout. AT1006 can measure the change in the capacitance of both sensors together and MS3110 can read only one sensor output at a time. And the displacement comb drive shows the sum of load cell beams deflection and the deformation in the specimen from which we can calculate the strain.

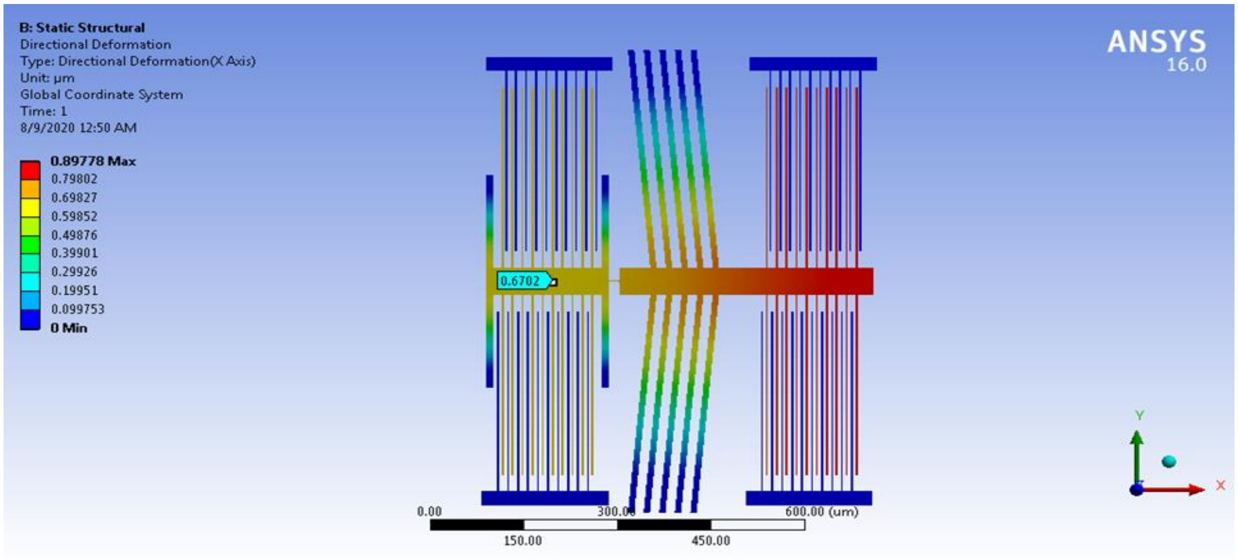

Figure 3.15: Displacements along the x-axis for the uniaxial machine at applied voltage 0.07V (a) the nickel specimen.

3.3.2 Equivalent Stress (Von-Mises) for Uniaxial Tensile Testing Machine

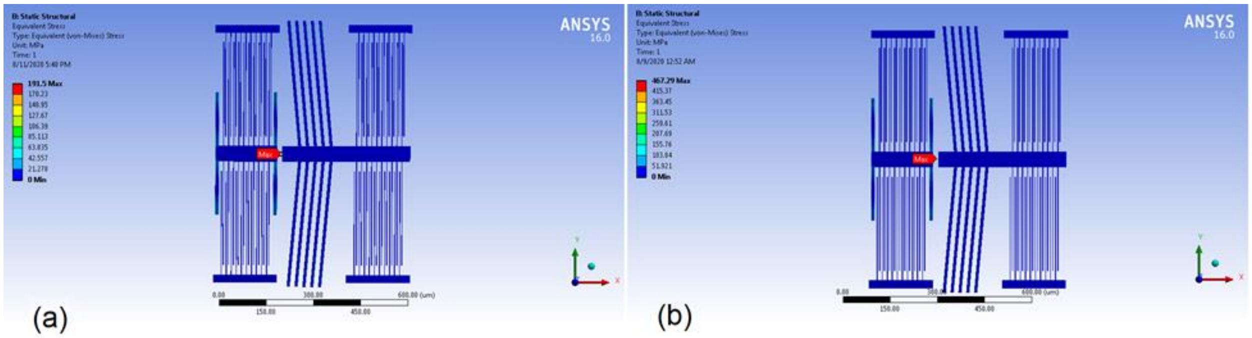

Figure 3.16: Comparison of equivalent (Von-Mises) stresses for the uniaxial machine at applied voltage 0.05V for (a) the gold specimen and for 0.07V for (b) the nickel specimen.

The equivalent stresses developed in both the gold and the nickel specimens are shown against the applied voltages 0.05V and 0.07V respectively. Nonlinear behaviors are observed in both cases showing the transition of the specimen from the elastic to the plastic region.

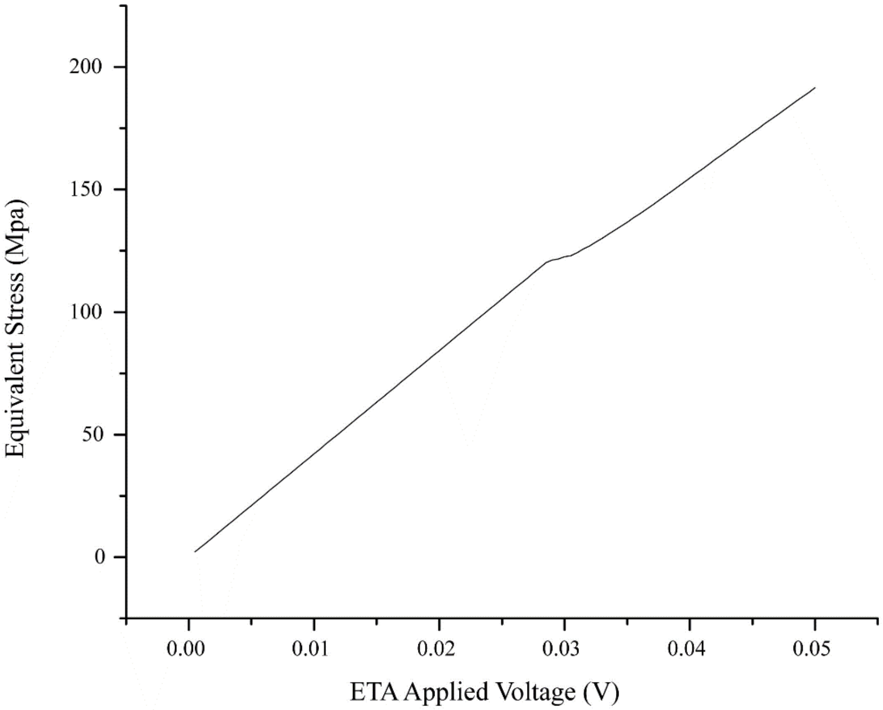

Figure 3.17: Equivalent (Von-Mises) stress versus applied voltage for the gold specimen.

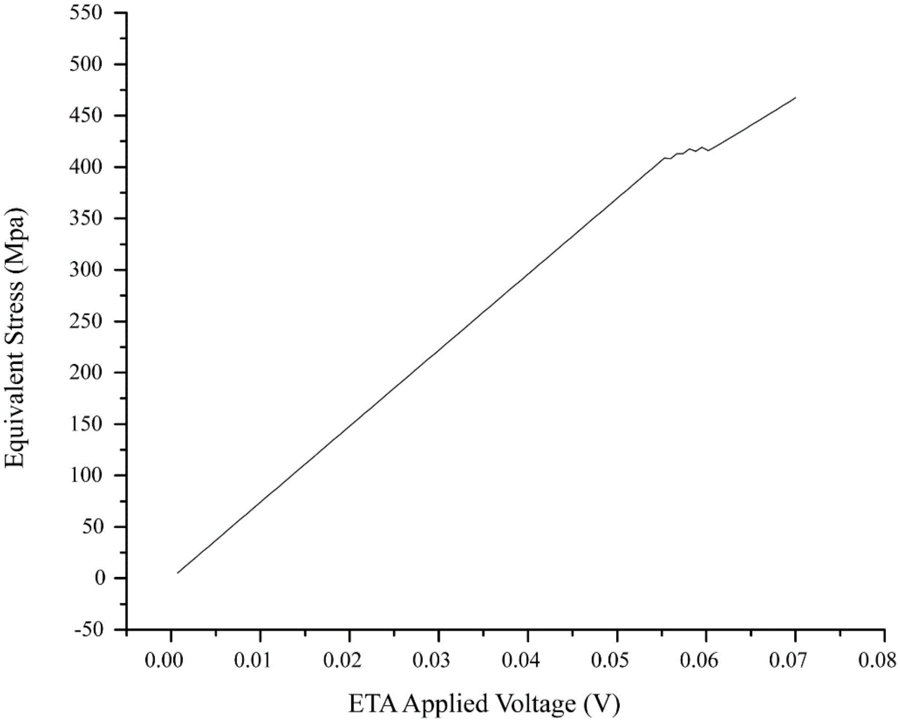

Figure 3.18: Equivalent (Von-Mises) stress versus applied voltage for the nickel specimen.

3.3.3 Equivalent Total Strain for Uniaxial Tensile Testing Machine

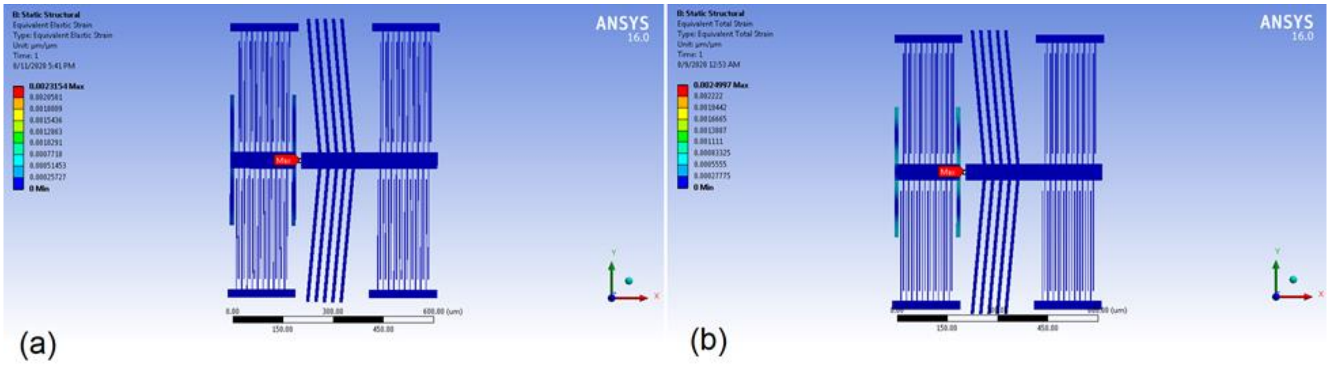

Figure 3.19: Equivalent total strain at the applied voltage 0.05V for (a) the gold specimen and at 0.07V applied voltage for (b) the nickel specimen.

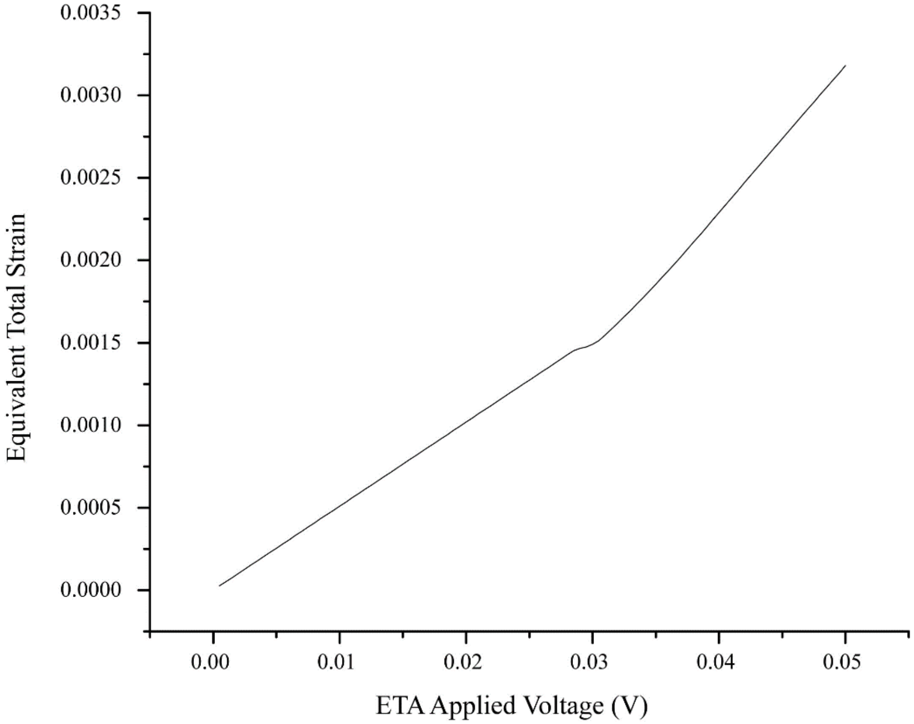

Figure 3.20: Equivalent total strain versus applied voltage for the gold specimen.

From the graphs of equivalent stress and equivalent total strain and the applied voltages for both the gold and the nickel specimen in figure 3.17, figure 3.18, figure 3.20 and figure 3.21 that a sudden change in both stress and strain appear when the material entering elastic to the plastic region [8].

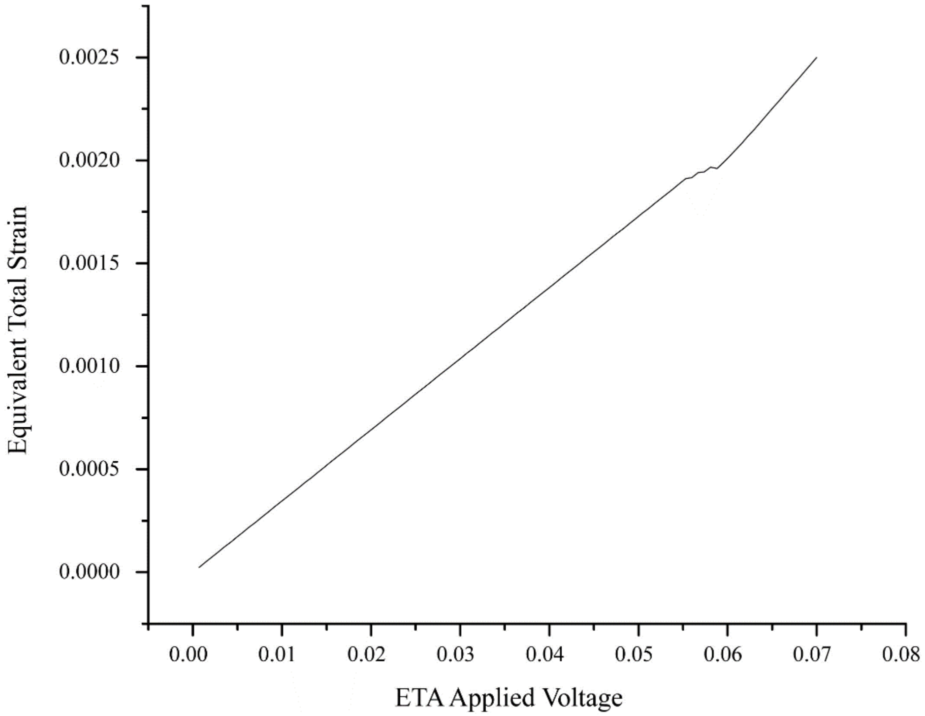

Figure 3.21: Equivalent total strain versus applied voltage for the nickel specimen.

3.4 Engineering Graph of Gold and Nickel for Uniaxial Tensile Testing Machine

From the FEM analysis values of equivalent stress and total equivalent strain, a graph is drawn to predict the yield strength of the materials. A similar graph has shown for biaxial design a linear region up to a certain value of stress after the nonlinear behavior is developed and the slope of the graph change. The point where this nonlinearity is developed is the yield strength of the material and the corresponding stress is known as yield stress of the material [8].

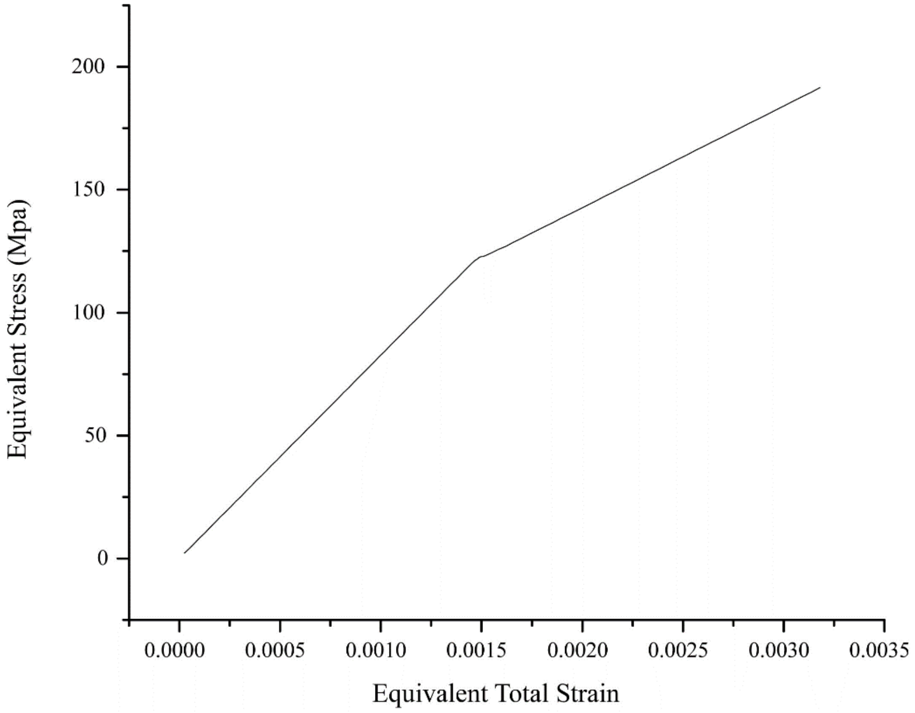

Figure 3.22: Equivalent total stress versus equivalent total strain the gold specimen.

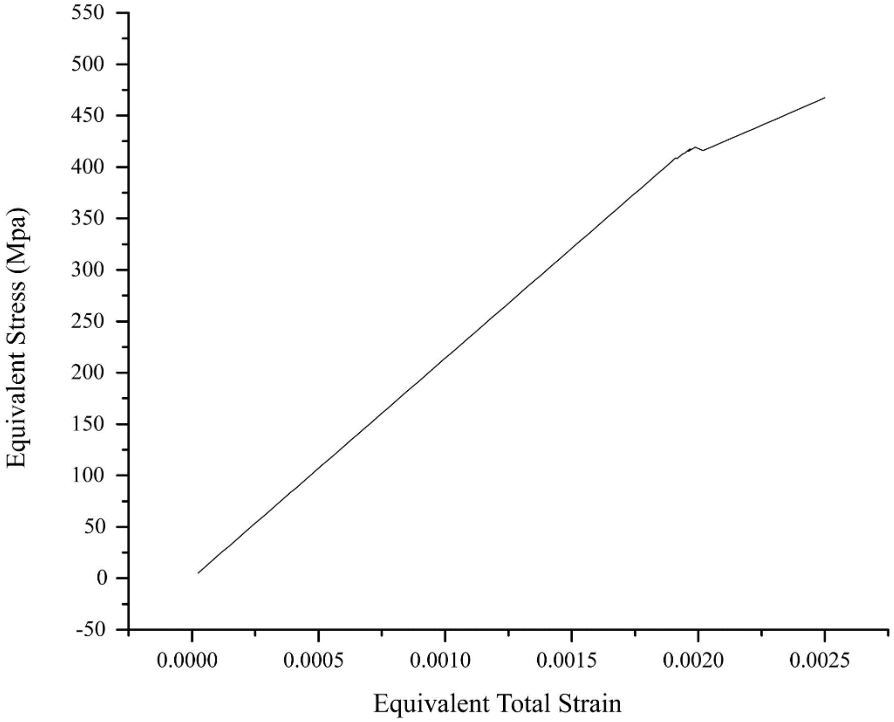

Figure 3.23: Equivalent total stress versus equivalent total strain the nickel specimen.

Chapter 4: Conclusion

The two new designs are proposed to find the yield strength of different MEMS materials in different sizes. The first design is used for the biaxial tensile testing of different materials in a variety of sizes. It consists of two electrothermal actuators of the nickel designed in such a way that they produce maximum output force and the small displacement at low input power as desired in tensile testing. The gold and the nickel specimens of 10 μm × 2 μm × 5 μm size with known properties are used as the test cases to check the design accuracy. First, for the gold specimen, the actuators were powered with 0.05V, and change in deflection sensors were monitored closely with the help of an additional electronics circuit. A smooth change in the capacitance was observed up to a certain point and then an abrupt change was observed at a certain. That is the point where material entering from the elastic to the plastic region and corresponding stress which is the yield stress of the gold specimen was found the same as given in the material properties for the analysis. Similarly, for the nickel specimen, it was also found the same as in the material properties. The temperature rise in both the specimens was found only found $39.71°C$ which has an almost negligible effect on the material properties. The second design used a uniaxial technique for tensile testing and has only one electrothermal actuator of nickel with the same geometry as in biaxial one. Additionally, it has one load cell and the specimen was mounted in between the load cell and the actuator. Both the gold and the nickel specimens were used as test cases. And the yield points of the gold and the nickel specimens were achieved for the applied voltages of 0.05V and 0.07V at the temperature rises of $26.34°C$ and $36.29°C$ respectively. The yield stresses were found directly from the design almost the same as given in their material properties for the analysis. It was found with help of ANSYS16.1 analyses that both the design has high accuracy at very low input power and small change in the temperature of the specimen as compared to the existing design discussed in the literature review. Additionally, they are easy to fabricate and can test a variety of materials for different sizes. We can easily redesign the systems just by increasing the actuator output force in case of biaxial design and actuator output force and load cell beams spring constants to use these for the material having high yield strengths like silicon or vice versa. All these make them attractive systems for tensile testing both at micron and submicron levels.

4.1 Future Work

This research work has covered only the mechanical part of the testing machines and the supportive electronics part is for future research work.

References

[1] R. C. Jaeger, *Introduction to microelectronic fabrication*. Prentice Hall Upper Saddle River, NJ, 2002.

[2] H. C. Nathanson, W. E. Newell, R. A. Wickstrom, and J. R. Davis, "The resonant gate transistor," *IEEE Transactions on Electron Devices,* vol. 14, no. 3, pp. 117-133, 1967.

[3] R. Howe and R. Muller, "Polycrystalline silicon micromechanical beams," *Journal of the Electrochemical Society,* vol. 130, no. 6, p. 1420, 1983.

[4] C. Liu, *Foundations of MEMS*. Pearson Education India, 2012.

[5] G. M. Rebeiz, *RF MEMS: theory, design, and technology*. John Wiley & Sons, 2004.

[6] U. Schmitt, "Knowcations-A meme-based personal knowledge management system-in-progress," in *Proceedings of the 8th International Conference on e-Learning ICEL, ACPI*, 2013, pp. 523-527.

[7] A. B. Pereira, F. A. Fernandes, A. B. de Morais, and J. Maio, "Biaxial Testing Machine: Development and Evaluation," *Machines,* vol. 8, no. 3, p. 40, 2020.

[8] Y. Zhang and J. Zhang, "Sintering phenomena and mechanical strength of nickel based materials in direct metal laser sintering process--a molecular dynamics study," *Journal of Materials Research,* vol. 31, no. 15, p. 2233, 2016.

[9] T. Tsuchiya, O. Tabata, J. Sakata, and Y. Taga, "Specimen size effect on tensile strength of surface-micromachined polycrystalline silicon thin films," *Journal of Microelectromechanical Systems,* vol. 7, no. 1, pp. 106-113, 1998.

[10] M. Saif and N. MacDonald, "Microinstruments for submicron material studies," *Journal of materials research,* vol. 13, no. 12, pp. 3353-3356, 1998.

[11] M. A. Haque and M. T. A. Saif, "Application of MEMS force sensors for in situ mechanical characterization of nano-scale thin films in SEM and TEM," *Sensors and Actuators A: Physical,* vol. 97, pp. 239-245, 2002.

[12] I. Chasiotis and W. G. Knauss, "Microtensile tests with the aid of probe microscopy for the study of MEMS materials," in *Materials and Device Characterization in Micromachining III*, 2000, vol. 4175: International Society for Optics and Photonics, pp. 96-103.

[13] M. A. Haque and M. Saif, "Microscale materials testing using MEMS actuators," *Journal of Microelectromechanical Systems,* vol. 10, no. 1, pp. 146-152, 2001.

[14] Y. Isono, T. Namazu, N. Terayama, and T. Tanaka, "Mechanical characterization of sub-micrometer thick DLC films by AFM tensile testing for surface modification in MEMS," in *Technical Digest. MEMS 2002 IEEE International Conference. Fifteenth IEEE International Conference on Micro Electro Mechanical Systems (Cat. No. 02CH37266)*, 2002: IEEE, pp. 431-434.

[15] T. Tsuchiya, "Tensile testing of MEMS materials," in *The 13th International Conference on Solid-State Sensors, Actuators and Microsystems, 2005. Digest of Technical Papers. TRANSDUCERS'05.*, 2005, vol. 2: IEEE, pp. 1953-1956.

[16] S. Han *et al.*, "Mechanical properties of Au thin film for application in MEMS/NENS using microtensile test," *Current Applied Physics,* vol. 6, pp. e81-e85, 2006.

[17] A. Desai and M. A. Haque, "Mechanical properties of ZnO nanowires," *Sensors and Actuators A: Physical,* vol. 134, no. 1, pp. 169-176, 2007.

[18] Y. Zhu, A. Corigliano, and H. D. Espinosa, "A thermal actuator for nanoscale in situ microscopy testing: design and characterization," *Journal of micromechanics and microengineering,* vol. 16, no. 2, p. 242, 2006.

[19] H. D. Espinosa, Y. Zhu, and N. Moldovan, "Design and operation of a MEMS-based material testing system for nanomechanical characterization," *Journal of Microelectromechanical Systems,* vol. 16, no. 5, pp. 1219-1231, 2007.

[20] J. H. Han, J. Rajagopalan, and M. T. A. Saif, "MEMS-based testing stage to study electrical and mechanical properties of nanocrystalline metal films," in *MEMS/MOEMS Components and Their Applications IV*, 2007, vol. 6464: International Society for Optics and Photonics, p. 64640C.

[21] M. Naraghi, I. Chasiotis, H. Kahn, Y. Wen, and Y. Dzenis, "Novel method for mechanical characterization of polymeric nanofibers," *Review of scientific instruments,* vol. 78, no. 8, p. 085108, 2007.

[22] Q. Jin, T. Li, Y. Wang, X. Li, P. Zhou, and F. Xu, "In-situ TEM tensile test of 90nm-thick< 110> SCS beam using MEMS chip," in *SENSORS, 2008 IEEE,* 2008: IEEE, pp. 1116-1118.

[23] J.-E. Ha, J.-H. Park, and D.-J. Kang, "New strain measurement method at axial tensile test of thin films through direct imaging," *Journal of Physics D: Applied Physics,* vol. 41, no. 17, p. 175406, 2008.

[24] R. Liu, H. Wang, X. Li, J. Tang, S. Mao, and G. Ding, "Analysis, simulation and fabrication of MEMS springs for a micro-tensile system," *Journal of Micromechanics and Microengineering,* vol. 19, no. 1, p. 015027, 2008.

[25] J. J. Brown *et al.*, "Microsystem for nanofiber electromechanical measurements," *Sensors and Actuators A: Physical,* vol. 155, no. 1, pp. 1-7, 2009.

[26] F. Schneider, T. Fellner, J. Wilde, and U. Wallrabe, "Mechanical properties of silicones for MEMS," *Journal of Micromechanics and Microengineering,* vol. 18, no. 6, p. 065008, 2008.

[27] J. r. Schröder and K. Görsch, "Storage Stability and Material Compatibility of Poly (oxymethylene) Dimethyl Ether Diesel Fuel," *Energy & Fuels*, vol. 34, no. 1, pp. 450-459, 2019.

[28] Y. Ganesan, Y. Lu, C. Peng, H. Lu, R. Ballarini, and J. Lou, "Development and application of a novel microfabricated device for the in situ tensile testing of 1-D nanomaterials," *Journal of microelectromechanical systems,* vol. 19, no. 3, pp. 675-682, 2010.

[29] W. Kang, J. H. Han, and M. T. A. Saif, "A novel method for in situ uniaxial tests at the micro/nanoscale—Part II: Experiment," *Journal of microelectromechanical systems,* vol. 19, no. 6, pp. 1322-1330, 2010.

[30] A. Boe, A. Safi, M. Coulombier, D. Fabrègue, T. Pardoen, and J.-P. Raskin, "MEMS-based microstructures for nanomechanical characterization of thin films," *Smart Materials and Structures,* vol. 18, no. 11, p. 115018, 2009.

[31] Y. Zhang *et al.*, "A MEMS tensile testing device for mechanical characterization of individual nanowires," in *SENSORS, 2010 IEEE*, 2010: IEEE, pp. 2581-2584.

[32] Y. Lu, C. Peng, Y. Ganesan, J. Y. Huang, and J. Lou, "Quantitative in situ TEM tensile testing of an individual nickel nanowire," *Nanotechnology,* vol. 22, no. 35, p. 355702, 2011.

[33] J. Brown, A. Baca, K. A. Bertness, D. Dikin, R. Ruoff, and V. M. Bright, "Tensile measurement of single crystal gallium nitride nanowires on MEMS test stages," *Sensors and Actuators A: Physical,* vol. 166, no. 2, pp. 177-186, 2011.

[34] Z. Hong-Jiang, L. Tie, J. Qin-Hua, X. Fang-Fang, and W. Yue-Lin, "Determination of the lattice parameters of a Si nanobelt in a tensile test process using an MEMS actuator," *Chinese Physics Letters*, vol. 29, no. 12, p. 126101, 2012.

[35] K. Abbas, S. Alaie, and Z. C. Leseman, "Design and characterization of a low temperature gradient and large displacement thermal actuators for in situ mechanical testing of

nanoscale materials," *Journal of Micromechanics and Microengineering,* vol. 22, no. 12, p. 125027, 2012.

[36] T. Tsuchiya, Y. Ura, K. Sugano, and O. Tabata, "Electrostatic Tensile Testing Device With Nanonewton and Nanometer Resolution and Its Application to $\hbox {C} _ {60} $ Nanowire Testing," *Journal of microelectromechanical systems,* vol. 21, no. 3, pp. 523-529, 2012.

[37] M. Yilmaz and J. W. Kysar, "Monolithic integration of nanoscale tensile specimens and MEMS structures," *Nanotechnology,* vol. 24, no. 16, p. 165502, 2013.

[38] T.-H. Chang and Y. Zhu, "A microelectromechanical system for thermomechanical testing of nanostructures," *Applied Physics Letters,* vol. 103, no. 26, p. 263114, 2013.

[39] M. F. Pantano, R. A. Bernal, L. Pagnotta, and H. D. Espinosa, "Multiphysics design and implementation of a microsystem for displacement-controlled tensile testing of nanomaterials," *Meccanica,* vol. 50, no. 2, pp. 549-560, 2015.

[40] S. Gupta and O. N. Pierron, "A MEMS tensile testing technique for measuring true activation volume and effective stress in nanocrystalline ultrathin microbeams," *Journal of Microelectromechanical Systems,* vol. 26, no. 5, pp. 1082-1092, 2017.

[41] A. M. Beese, D. Papkov, S. Li, Y. Dzenis, and H. D. Espinosa, "In situ transmission electron microscope tensile testing reveals structure–property relationships in carbon nanofibers," *Carbon,* vol. 60, pp. 246-253, 2013.

[42] T. Tsuchiya, T. Hemmi, J.-y. Suzuki, Y. Hirai, and O. Tabata, "Tensile strength of silicon nanowires batch-fabricated into electrostatic MEMS testing device," *Applied Sciences,* vol. 8, no. 6, p. 880, 2018.

[43] C. Howard, C. Judge, and P. Hosemann, "Applying a new push-to-pull micro-tensile testing technique to evaluate the mechanical properties of high dose Inconel X-750," *Materials Science and Engineering: A,* vol. 748, pp. 396-406, 2019.

[44] Z. Zhang, W. Zhang, Q. Wu, Y. Yu, X. Liu, and X. Zhang, "Closed-form modelling and design analysis of V-and Z-shaped electrothermal microactuators," *Journal of Micromechanics and Microengineering,* vol. 27, no. 1, p. 015023, 2016.

[45] M. Saqib, M. M. Saleem, S. U. Awan, and M. U. Rehman, "Design, Modeling and Parametric Analysis of Chevron Shaped Electrothermal Actuator Using Low Cost MetalMUMPS Fabrication Process," in *2018 International Conference on Computing, Electronic and Electrical Engineering (ICE Cube)*, 2018: IEEE, pp. 1-5.

[46] D. Yan, A. Khajepour, and R. Mansour, "Modeling of two-hot-arm horizontal thermal actuator," *Journal of Micromechanics and Microengineering,* vol. 13, no. 2, p. 312, 2003.

[47] W. Suocheng, H. Yongping, and L. Shuangjie, "The design and analysis of a MEMS electrothermal actuator," *Journal of Semiconductors,* vol. 36, no. 4, p. 044012, 2015.

[48] M. Saqib, M. Mubasher Saleem, N. Mazhar, S. U. Awan, and U. Shahbaz Khan, "Design and analysis of a high-gain and robust multi-DOF electro-thermally actuated MEMS gyroscope," *Micromachines,* vol. 9, no. 11, p. 577, 2018.

[49] Z. Zhang, Y. Yu, X. Liu, and X. Zhang, "Dynamic modelling and analysis of V-and Z-shaped electrothermal microactuators," *Microsystem Technologies,* vol. 23, no. 8, pp. 3775-3789, 2017.

[50] L. Li and D. Uttamchandani, "Dynamic response modelling and characterization of a vertical electrothermal actuator," *Journal of Micromechanics and microengineering,* vol. 19, no. 7, p. 075014, 2009.

[51] R. Mukhiya *et al.*, "Design, modelling and system level simulations of DRIE-based MEMS differential capacitive accelerometer," *Microsystem Technologies,* vol. 25, no. 9, pp. 3521-3532, 2019.

[52] S. Chung and S. Park, "Effects of temperature on mechanical properties of SU-8 photoresist material," *Journal of Mechanical Science and Technology,* vol. 27, no. 9, pp. 2701-2707, 2013.

[53] L. Kren, "ONE AXIS--ONE CHIP," *Machine Design*, vol. 73, no. 10, pp. 42-42, 2001.

[54] G. Coffin, "Digital Modelling (AT1006): Produce a High Quality Photo Realistic 3D Computer Model," University of Wolverhampton, 2008.

Completion Certificate

It is certified that the contents of the thesis document titled "***Design of a MEMS Based Universal Testing Machine for Thin Film Characterization***" submitted by NS Arslan Ul Haq, Registration No. 00000171745 have been found satisfactory in all respects as per the requirements of Main Office, NUST (Exam branch).

Supervisor: ___________________
Dr. Muhammad Mubasher Saleem
Date: ____ August 2020